Eur. Phys. J. D **41**, 25–47 (2007)
DOI: 10.1140/epjd/e2006-00193-0

THE EUROPEAN PHYSICAL JOURNAL D

Isotope shifts and accurate wavelengths in Ne II and Ne III*

K.J. Öberg[a]

Atomic Astrophysics, Lund Observatory, Box 43, 221 00 Lund, Sweden

Received 31 March 2006 / Received in final form 9 June 2006
Published online 18 August 2006 –

Abstract. Transition isotope shifts of 3s–3p transitions in Ne II and Ne III are measured in Fourier transform spectra from a hollow-cathode source. Accurate absolute line-center positions of the ^{20}Ne isotope are derived for the purpose of tertiary wavelength standards in the region 2000–5000 Å. A robust statistical treatment is applied, yielding line-position uncertainties that are lower than for the Ar II secondary standards used as references. The influence of Stark shifts on both the new Ne II standards and the Ar II standards is also investigated. In addition, improved wavenumbers of the 3p–3d and 3p–4s transitions are presented, of which 12 in Ne II have been measured for the first time.

PACS. 32.30.Jc Visible and ultraviolet spectra – 32.60.+i Zeeman and Stark effects – 32.70.Jz Line shapes, widths, and shifts

1 Introduction

Neon is a common buffer gas in spectroscopic light sources, such as hollow-cathode (HC) and Penning lamps. The glow discharge in these sources produces strong spectral lines of both the cathode material and the buffer gas, from neutral to doubly ionized. This makes it possible to use neon transitions as internal wavelength standards for all other spectral lines emitted from the same plasma. However, for high accuracy measurements between 2000 and 5000 Å the available data on neon are not sufficient. Wavelength uncertainties are too high and isotope effects must be considered. The most appropriate calibration lines in this region are the 3s–3p transitions of Ne II, since they are strong and the least sensitive to Stark shifts [1]. These transitions are all affected by isotope shifts (IS) and no prior studies have taken this into account quantitatively when determining the positions. In this work, thorough deconvolutions of the 3s–3p line profiles are performed, yielding both IS between ^{20}Ne and ^{22}Ne and accurate wavenumbers of the dominant ^{20}Ne isotope.

Neon has three naturally occurring isotopes, $^{20-22}$Ne, with the atmospheric concentrations of 90.48%, 0.27% and 9.25%, respectively [2]. There are a number of published studies on the IS of the 3s–3p transitions of Ne II. The most complete was done by Murakawa [3], who studied spectra from a liquid-air cooled tungsten HC with the etalon interference technique. He determined the IS of 14 transitions with relative uncertainties as low as 3% for the largest shifts. Some of these were later remeasured by Kreye [4], but at lower accuracy. In the present work the IS of 45 Ne II 3s–3p transitions are presented, with uncertainties about an order of magnitude lower than those in [3]. There is no prior experimental study of the IS in Ne III, and the 41 values presented here are measured for the first time. In addition, the IS for some of the 3s–4p and 3s–5p transitions of Ne II has also been measured.

Kramida and Nave have compiled and evaluated most of the previous work on line positions of Ne II and Ne III [5,6]. In these two extensive works, they improve energy levels from which Ritz wavelengths are derived, however, the influence of IS is not regarded. To the most accurate Ne II and Ne III 3s–3p transitions they assign an uncertainty of about 0.002 and 0.004 cm^{-1}, respectively, which is roughly the size of shifts from the ^{20}Ne line center positions if the IS is not taken into account in an unresolved profile. When energy levels are fitted, these shifts influence Ritz wavelengths of lines without visible IS. With uncertainties one order of magnitude lower in the present work, this motivates an investigation of transitions from further up in the system than the 3p levels.

The neon spectra used in this work, recorded over a wide range of discharge conditions, are calibrated with the Ar II secondary standards of Whaling et al. [7]. A robust statistical method is applied, resulting in uncertainties of the 3s–3p Ne II line center positions of ^{20}Ne that are lower than those stated for the Ar II standards. The Ritz wavenumbers of these neon transitions are recommended as tertiary standards for high accuracy measurements. For both the Ar II and the new Ne II standards, it is demonstrated that Stark shifts in the HC plasma set the limit to the accuracy of a calibration.

* Supplementary files concerning Ritz wavenumbers and the associated uncertainties are only available in electronic form at `http://www.eurphysj.org`.

[a] e-mail: `kasper@astro.lu.se`

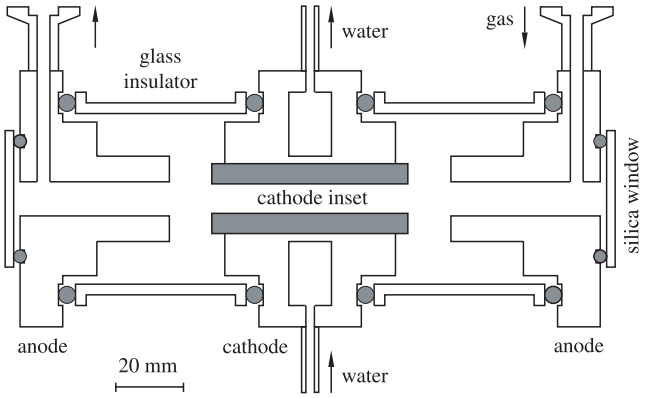

Fig. 1. The HC source used in the investigation. Anodes and cathode are of stainless steel. Figure by courtesy of Ulf Litzén.

2 Experimental set-up

Spectra were recorded with a Chelsea Instruments FT500 Fourier transform spectrometer (FTS) [8]. This instrument has a high-resolution coverage of the region 2000–7000 Å, where most of the 3s–3p transitions of Ne II and Ne III are located. The instrument provides double-sided interferograms, which are less sensitive than single-sided to error in line-center positions due to phase corrections [9]. To transform the interferograms, the FTS data-analysis program Xgremlin [10] was used.

Spectral lines of neon were produced with a water-cooled HC source with replaceable cathode insets, see Figure 1. These have a cylindrical bore 54 mm in length that confines the glow-discharge plasma. Both sides of the bore are open and the anodes, centered on the same axis as the cathodes, are positioned about 18 mm away on each end. When viewed through the centre of the anodes, the discharge plasma has a 180-degree rotational symmetry around any axis that goes through its centre and is perpendicular to the line of sight. By this geometry, the atoms and ions have no preferred direction along the central axis. Doppler effects, such as diffusion and ions accelerating towards the cathode walls, will therefore have a negligible influence on the positions of spectral lines that are unaffected by self-absorption. However, diffusion will result in asymmetric line profiles if self-absorption is present, since photons emitted from the far end of the plasma have a higher probability to be absorbed.

A quartz lens with a focal length of 75 mm was used to collimate the light from the plasma. It was placed at a distance of 150 mm from the aperture of the FTS. The bore of the HC was placed within one and two focal lengths on the opposite side of the lens, with the focal point close to the opening of the bore. From this setup, the image of the plasma upon the aperture will be diffuse and most of the light will come from the central parts of the plasma. This was done in order to avoid wavenumber shifts due to an unevenly illuminated aperture [11]; and also to minimize light from the cathode walls, where strong electrical fields can cause Stark shifts. Great care was also taken to align the light source and the lens with the optical path of the instrument.

Three cathodes, containing more than 99.5% pure aluminum, with a bore of 3, 6 and 9 mm in diameter, were used in the investigation. This was done to see if the diameter influences the absolute positions of the spectral lines. Further, a 6 mm titanium cathode, 99.99% pure, was used to detect and study neon lines blended with aluminum.

Aluminum was chosen for several reasons. It has a simple spectrum, making it easier to remove strong lines with optical filters, thereby decreasing the overall noise level of the spectra. In FTS recordings the photon noise of each line is distributed over the whole spectrum. The low line density also decreases the risk of having neon lines blended with metal lines.

Another good feature of aluminum cathodes is the low sputtering yield [12], which is the number of atoms per unit time emitted from the cathode walls. The sputtered atoms and electrons heat the plasma by collisions with the buffer gas atoms. Aluminum also has a high thermal conductivity and a cathode of this material is therefore efficient in cooling the plasma. This, in conjunction with the low sputtering yield, gives small Doppler widths of the gas lines, which makes it possible to resolve the IS of the 3s–3p transitions of Ne II and Ne III. Under the same discharge conditions, i.e. the same bore diameter, gas pressure and current, neon lines from the HC with the titanium inset have a 30% larger Doppler width than with the aluminum inset.

About a third of the 48 spectra were recorded for diagnostic purposes of the light-source. The remainder were used in the analysis of neon, 17 spectra in the region 2500–5000 Å (**A**) and 12 in 1900–3500 Å (**B**), detected with Hamamatsu R955 and R166 PM tubes, respectively. In the visible, the dominating spectral lines with the aluminum cathode are the 3s–3p transitions of Ne I and the resonance lines of Al I. They have intensities orders of magnitude stronger than the spectral lines of ionized neon. Even though being outside the first spectral region **A**, the 3s–3p transitions of Ne I contribute to the noise level, since the R955 is sensitive up to 8000 Å. To remove this effect Schott colored optical glass filters, BG24, were used. Spectra were also recorded with the narrower UG2 filter to lessen the influence of the 3944 and 3962 Å Al I resonance lines. Both filters decreased the noise level significantly, especially the latter. In the second spectral region **B** no filters were used, since R166 is solar blind and has a low sensitivity above 2800 Å. When recording a spectrum, several scans with the FTS were added together to further increase the S/N. The lowest number of scans per spectrum was 22, the highest 134.

To detect possible Stark shifts, induced by small-scale electrical fields from charged particles and atoms in the plasma, or external fields from the cathode walls, the discharge parameters were varied over a wide range. For all three diameters of the aluminum cathode, spectra were recorded with currents from 0.05 to 1.65A DC, with buffer gas pressures between 0.05 and 2.00 torr. The high purity neon was provided with a commercially available bottle, coupled in series with the HC and a turbo-molecular pump. The gas pressure was held constant when recording

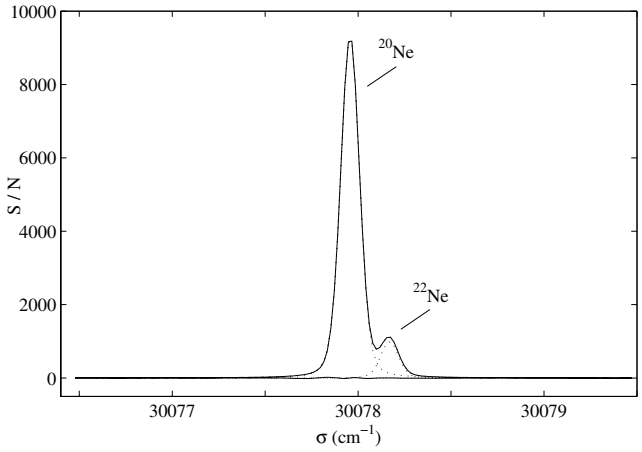

Fig. 2. The 30077.9803 cm^{-1} Ne II 3s–3p transitions recorded from a 0.05 A and 0.29 torr pure neon HC discharge. Solid line – observed data and residual; dotted – least-squares fit of a sum of two Voigt functions. The line profile has a $\delta\sigma_D/IS$ of 0.495.

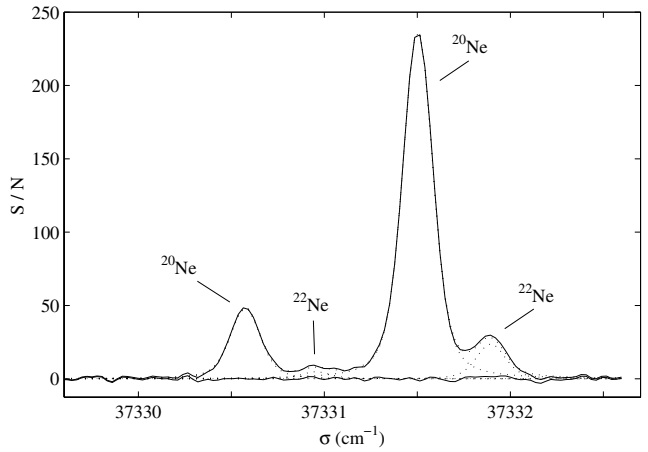

Fig. 3. The 37330.605 and 37331.5326 cm^{-1} Ne III 3s–3p transitions recorded from a 0.60 A and 0.90 torr pure neon HC discharge. Solid line – observed data and residual; dotted – simultaneous fit of the two transitions. The individual line profiles have a $\delta\sigma_D/IS$ of 0.40 and 0.385, respectively. The wavenumber scale is the same as in Figure 2.

data, monitored with a capacitance manometer. Argon was added to a level of 2–20% to make wavelength calibration in region **A** possible.

3 Neon line profiles

Using a BALZERS QMA125 quadrupole mass spectrometer, the ^{22}Ne/ ^{20}Ne isotope abundance ratio was determined to be 0.097 (0.001) and ^{21}Ne/ ^{22}Ne to be 0.027 (0.001). These deviate from the ratios, 0.102 and 0.029, respectively, calculated with the representative isotope composition of [2]. This indicates a mass dependence when neon is separated from air, i.e. the composition may vary between different bottles and manufacturers.

All 3s–3p Ne II and Ne III transitions with $S/N > 30$ show structure due to IS. Only the two components from the ^{20}Ne and ^{22}Ne isotopes are visible in the line profiles due to the low abundance of the odd isotope, see Figures 2 and 3. Individual isotope components and lines without structure have Voigt profiles, i.e. a convolution of a Gaussian and Lorentzian. The former comes from the thermal motion of the ions and the latter from the combined effect of natural and Stark broadening. From the recorded spectra it is clear that the Doppler widths of the Gaussians increase with the current, with typically 4.5 to 6 independent data points per FWHM. Lorentzian widths also increase with current, but not pressure, indicating Stark broadening by electrons. A term dependence was found for these widths, where transitions with an upper 3p ^{2}P° level are the least sensitive, see further Section 6.

For all strong 3s–3p transitions, the area ratios between the isotope components are larger than 0.097. This is expected if self-absorption is present, since the ^{20}Ne component is affected more than the weaker ^{22}Ne. For lines with $S/N > 500$, the ratios vary typically from 0.101 to 0.104, with relative uncertainties below one percent. Transitions within the same multiplet show similar ratio changes between different recorded spectra. However, no simple dependence on current or pressure was observed. A plausible explanation to the self-absorption is that the 2p–3s resonance photons are trapped within the discharge plasma, thereby drastically increasing the population of the 3s levels. Self-absorption of the 3s–3p transitions in Ne II has also been observed in other HC studies, see e.g. [13].

It was shown in [14], using Doppler-free two-photon spectroscopy on a 3s–4d transition in Ne I, that the mass-shift part of the IS is at least two orders of magnitude larger than the field shift. If a zero field shift is assumed, this gives the ratio [15]

$$(\sigma_{21} - \sigma_{20})/(\sigma_{22} - \sigma_{20}) = 0.5248. \quad (1)$$

By this relation, the position of the ^{21}Ne relative to the two other isotopes is known and it can be included in the fitting, even if it is not visible. For well-resolved strong transitions, this leaves a distinct negative trace in the residual at the position of the of ^{21}Ne component of roughly the same amplitude as the ^{21}Ne intensity. However, when it is not included in a fit, the residual is smaller without any distinct trace of ^{21}Ne detectable. This shows that the intensity of ^{21}Ne has been dispersed, which can be explained by the fact that transitions in odd isotopes are influenced by hyperfine structure (hfs), i.e. divided into several components. Therefore, only two components, representing ^{20}Ne and ^{22}Ne, were used when modeling the line structure.

4 Data analysis

4.1 Line profile fitting

The convolution of a Gaussian and Lorentzian, i.e. the Voigt profile, cannot be evaluated analytically.

Schreier [16] has investigated the relative errors of a number of approximations to the Voigt function. Among these, he recommends the fast and accurate algorithm of Humlíček [17], which is used in this work.

A set of line fitting routines were written, based on the Levenberg-Marquardt least-squares algorithm [18] and a sum of two Voigt functions. The Doppler width of the ^{22}Ne component was multiplied by a factor 0.953 to compensate for the heavier mass of this isotope. Since both components share the same transition, the Lorentzian widths were set to be the same.

To obtain the IS of the 3s–3p transitions, three routines were written with the shift as a free parameter: (i) the first routine had the area ratio of the isotope components as a free parameter, and was used when fitting strong transitions where self-absorption was evident. (ii) The second routine had the areas locked to the isotope ratio from the mass-spectrometer measurement. (iii) In the Ne III spectrum, three pairs of 3s–3p transitions were blended with each other. The best resolved is shown in Figure 3. To deconvolve these, the third routine was written, based on a sum of two profiles with free shifts and locked area ratios between its isotope components. The Doppler and Lorentzian widths were all set to the same, since the wavelengths are nearly the same and the transitions belong to the same multiplet. To determine the absolute positions of the 3s–3p transitions, another three routines were written. In all regards, these were the same as the previous three, except that the shifts were held constant.

A routine for fitting a pure Voigt profile was also written to investigate lines without structure, such as the Ar II calibration lines and non-3s–3p neon transitions. The line centers of the latter were assumed to be the positions of the ^{20}Ne component. For lines with $S/N < 20$, the wings are not well defined and a pure Gaussian profile was used.

For each spectrum, a global noise level was determined as the standard deviation in 20 evenly-spaced intervals free from spectral lines. This noise level was used in the weights of the curvature matrices of the routines described above. Uncertainties of the line parameters were then derived directly from the covariance matrices from the fitting of the lines.

4.2 Energy level fitting

A routine for simultaneously fitting an energy levels system to observed transitions was written, based on a weighted least-squares method. The linear system is defined by

$$Ax \cong y, \tag{2}$$

where the $m \times n$ matrix A determines which two elements in the vector x, containing n level energies, that correspond to an observed wavenumber in the vector y of length m. If p and q are the positions of the lower and upper levels in x that correspond to the transition y_j, then A has the elements $a_{jp} = -1$ and $a_{jq} = 1$. All other elements of the row j are zero. To make the system non-singular, the ground state is considered fixed at zero value with a zero uncertainty and is not included in x. Therefore, for a resonance transition the element $a_{jp} = -1$ is not present in A.

The wavenumbers in y are weighted by the $m \times m$ diagonal error matrix

$$\Sigma_{ii} = k_1^2(u_i^2 + k_2^2). \tag{3}$$

Here, u_i is the uncertainty of the observed wavenumber y_i. The multiplicative factor k_1 is needed for a simultaneous modification of uncertainties that stretch over several orders of magnitude, while k_2 modifies uncertainties that are of the same size as k_2 or smaller. The same k_1 and k_2 are used for all transitions, representing a global correction for underestimated uncertainties and errors. The resulting least-squares solution of (2) is then

$$\hat{x} = (A^T \Sigma^{-1} A)^{-1} A^T \Sigma^{-1} y \tag{4}$$

with the $n \times n$ covariance matrix $C = (A^T \Sigma^{-1} A)^{-1}$. If there are several observed wavenumbers of the same transition, instead of first calculating a weighted mean they can all be included in y, which will give the same $\hat{x}$ and C. The residual of the least-squares solution is represented by $r = y - A\hat{x}$ and χ^2 of the system can then be written as

$$\chi^2 = r^T \Sigma^{-1} r. \tag{5}$$

The values of k_1 and k_2 in (3) are determined by increasing them until χ^2 equals the degrees of freedom of the system, i.e. $m - n$. Levels connected with only one transition to the rest of the system have no influence on the reduced χ^2, but the uncertainties are modified in just the same way, following the assumption of a global error.

The uncertainty of a fitted level energy $\hat{x}_i$ is given by square root of the diagonal element c_{ii} in the covariance matrix C. Ritz wavenumbers $\hat{y}$ of the observed transitions are simply calculated by

$$\hat{y} = A\hat{x}. \tag{6}$$

The uncertainty of $\hat{y}_i$ is given by the square root of the diagonal element v_{ii} in the $m \times m$ matrix

$$V = ACA^T. \tag{7}$$

By the appropriate choice of non-zero elements in a row vector a of length n, the Ritz wavenumbers of any transition, with its lower and upper levels present in $\hat{x}$, can be calculated by $a\hat{x}$. The uncertainty of this wavenumber is then given by the square root of the variance aCa^T. In the case of an observed transition that is included in y, the vector a corresponds to a row in A.

The least-squares fit of energy levels is based on the method proposed in [19]. It is here written in a simplified formalism and k_2 in the error matrix (3) is introduced. Also, a procedure to determine the values of k_1 and k_2 is presented, which, if the uncertainties of the observed wavenumbers are underestimated, makes the derived uncertainties consistent with the values of the Ritz wavenumbers.

4.3 Procedure

The starting parameters of each fit of a line profile were defined graphically by hand in a line-fitting program, incorporating the routines described in Section 4.1. Each individual fit was critically evaluated by eye and by the reduced χ^2. Great care was also taken to ensure that the diagonal factors $1 + \lambda$ of the curvature matrix in the Levenberg-Marquardt algorithm [18] approached unity.

The reason for having two sets of fitting routines, one with free and one with locked shifts, see Section 4.1, was to make a self-consistent analysis possible. With the first set the IS of each spectral line was determined. This was then held constant when applying the second set of routines, giving the absolute positions. If a large error was introduced in the first step of the analysis, it would show in the latter fitting.

In the derivation of the calibration factors α, see Section 5.2, the IS and the line center positions of the ^{20}Ne components, a modified weighted mean x_ϵ was applied. This mean is defined by

$$x_\epsilon = \frac{\sum_i^n x_i (u_i^2 + \epsilon^2)^{-1}}{\sum_i^n (u_i^2 + \epsilon^2)^{-1}}, \tag{8}$$

where the n individual measurements have values and estimated uncertainties represented by x_i and u_i, respectively. The associated variance u_ϵ^2 and χ_ϵ^2 are given by

$$u_\epsilon^2 = \frac{1}{\sum_i^n (u_i^2 + \epsilon^2)^{-1}} \tag{9}$$

and

$$\chi_\epsilon^2 = \sum_i^n \frac{(x_i - x_\epsilon)^2}{u_i^2 + \epsilon^2}. \tag{10}$$

When applying (8), an ordinary weighted mean x_{wm} is first calculated by setting ϵ to zero. If the resulting χ_ϵ^2 is lower than the degrees of freedom $n - 1$, the uncertainties of the individual measurements u_i may be overestimated. In this case the mean x_{wm} and the uncertainty u_{wm} are kept, even though the latter may be too large. However, if the reduced χ_ϵ^2 is greater than $n - 1$, the uncertainties u_i may be underestimated or an unmodeled error can be present. To compensate for this, the quantity ϵ is added in quadrature to all estimated uncertainties u_i in (8)–(10). The value of ϵ is determined by solving the equation $\chi_\epsilon^2 = n - 1$ and is then used to calculate new values of x_ϵ and u_ϵ. By studying the effect on χ_ϵ^2 when a measurement is added, unidentified blends or Stark shifts can be detected, and if not, the influence on the mean is to some extent incorporated in the uncertainty of the mean.

4.4 Effects of correlated noise in the FTS spectra

When deriving uncertainties of the line parameters as described in Section 4.1, they are true only if the noise in the data points of a line is white, which is not the case in the FTS spectra used in this work. This can be shown by calculating the autocovariance of a part of a spectrum with only noise, see e.g. [20], resulting in correlation coefficients ρ_1 at lag 1 of about 0.45 for all spectra. From this it can be shown that the global noise level has been underestimated by a factor of 1.4. The correlation coefficients at lag 2 and 3 are negative with values about -0.1, which should somewhat mitigate the effect.

Instead of further improving the analysis of the noise, the robust statistical methods presented in Sections 4.2 and 4.3 can be applied, which will compensate for the non-random noise. When fitting a line profile the uncertainty u_i of the position is proportional to $(S/N)^{-1}$. If the standard deviation of the noise in all spectra is multiplied with a factor of 1.4, this results in the same increase in all u_i. By setting the uncertainties of the reference wavenumbers to zero when calibrating, see Section 5.2, the uncertainty of the weighted mean of α is also increased by a factor of 1.4. From this, the change in uncertainty of a calibrated line is the same as for an uncalibrated. Further, the 1.4 factor propagates unchanged to the uncertainties of all weighted means u_{wm} of the calibrated lines. When these in turn are inserted in the error matrix (3), the factor is present in all elements of Σ.

Clearly, instead of multiplying the standard deviation of the noise with 1.4, k_1 can be set to this value in (3). If the analysis, based on the standard deviation of the noise only, results in k_1 that are greater than 1.4, the non-random noise has been compensated for. This statement is strengthened if the uncertainties of the reference wavenumbers are non-zero, and also if non-zero ϵ has been used in (8)–(10) before fitting the energy levels. Further, the noise correction with a factor of 1.4 is an overestimated compensation for the correlated noise. The uncertainty of the IS is also proportional to $(S/N)^{-1}$, and a similar argument can be used for this.

When fitting a spectral line using the least-squares routines described in Section 4.1, in contrast to the uncertainty, the value of the line center position is unaffected by rescaling of the noise. If the same scaling factor is used in several spectra, the weighted mean of wavenumbers belonging to the same transition is also preserved, as are the Ritz wavenumbers derived from these spectra. Non-zero ϵ and k_2 will, however, influence the values.

5 Results

5.1 Transition isotope shifts

Only transitions where 3s electrons are involved show line structure due to IS. All others have good residuals when fitted with a Voigt function. In all line profiles where ^{22}Ne could be discerned, its position was blue shifted relative to ^{20}Ne as expected from the normal mass shift. For the size of the shifts, there is a clear dependence on the terms involved, indicating specific mass shifts, see Tables 1 and 2. This can also be seen by simply calculating the normal mass shifts [15], which shows that all specific shifts are to higher wavenumbers. For the 3p–3d and 3p–4s transitions

Table 1. Transition isotope shifts in Ne II.

Transition[a]		σ^b	IS^c_{Ritz}	$u^{c,d}_{Ritz}$	$u^{d,e}_{wm}$	$u^{d,e}_{\epsilon}$	$(IS_{Ritz} - IS_{\epsilon})$	spec[f]	IS
Lower	Upper	(cm^{-1})	(10^{-3} cm^{-1})			(10^{-3} cm^{-1})			Ref. [3]
$(^3P)3s\ ^4P_{5/2}$	$(^3P)3p\ ^4P^\circ_{5/2}$	27061.6503	131.13	0.45	0.19	0.34	0.06	6	150 (15)
	$(^3P)3p\ ^4P^\circ_{3/2}$	27284.2513	132.24	0.45	0.18	0.33	0.14	11	148 (15)
	$(^3P)3p\ ^4D^\circ_{7/2}$	29977.8517	126.41	0.49	0.15	0.32	$< 10^{-2}$	9	143 (16)
	$(^3P)3p\ ^4D^\circ_{5/2}$	30315.2005	127.17	0.70	0.58	0.80	−1.3	10	
	$(^3P)3p\ ^4D^\circ_{3/2}$	30564.7426	127.6	0.84	4.9	4.9	1.3	6	
	$(^3P)3p\ ^4S^\circ_{3/2}$	33822.7560	121.0	1.5	1.1	1.1	0.4	15	
$(^3P)3s\ ^4P_{3/2}$	$(^3P)3p\ ^4P^\circ_{5/2}$	26543.9859	130.05	0.52	0.27	0.42	−0.09	13	150 (19)
	$(^3P)3p\ ^4P^\circ_{3/2}$	26766.5870	131.15	0.56	0.58	0.61	−1.2	12	
	$(^3P)3p\ ^4P^\circ_{1/2}$	26949.2541	131.87	0.50	0.21	0.33	0.09	11	149 (15)
	$(^3P)3p\ ^4D^\circ_{5/2}$	29797.5362	126.08	0.55	0.25	0.40	0.33	8	160 (16)
	$(^3P)3p\ ^4D^\circ_{3/2}$	30047.0782	126.60	0.75	0.37	0.60	0.52	12	
	$(^3P)3p\ ^4D^\circ_{1/2}$	30191.1911	125.5	1.6	3.5	5.2	0.8	4	
	$(^3P)3p\ ^2D^\circ_{5/2}$	31362.7243	126.8	12	9.1	9.1	−2.6	5	
	$(^3P)3p\ ^4S^\circ_{3/2}$	33305.0916	119.9	1.5	1.3	1.9	−1.8	15	
$(^3P)3s\ ^4P_{1/2}$	$(^3P)3p\ ^4P^\circ_{3/2}$	26467.5681	129.55	0.38	0.25	0.26	0.14	12	
	$(^3P)3p\ ^4P^\circ_{1/2}$	26650.2353	130.2	0.78	1.0	1.5	−1.7	13	
	$(^3P)3p\ ^4D^\circ_{3/2}$	29748.0594	125.00	0.80	0.42	0.74	−0.83	9	
	$(^3P)3p\ ^4D^\circ_{1/2}$	29892.1723	123.9	1.4	0.40	0.99	−0.03	11	
	$(^3P)3p\ ^4S^\circ_{3/2}$	33006.0728	118.3	1.5	2.3	4.1	3.9	12	
$(^3P)3s\ ^2P_{3/2}$	$(^3P)3p\ ^4D^\circ_{5/2}$	25358.9545	209.32	12	19	19	−11	1	
	$(^3P)3p\ ^2D^\circ_{5/2}$	26924.1426	210.10	0.38	0.095	0.25	$< 10^{-2}$	5	203 (8)
	$(^3P)3p\ ^2D^\circ_{3/2}$	27435.0885	211.95	0.52	0.31	0.59	−0.53	12	
	$(^3P)3p\ ^2S^\circ_{1/2}$	28711.4555	215.03	0.40	0.23	0.28	0.13	11	
	$(^3P)3p\ ^2P^\circ_{3/2}$	30077.9803	211.986	0.047	0.031	0.031	0.005	8	219 (6)
	$(^3P)3p\ ^2P^\circ_{1/2}$	30205.1606	213.12	0.21	0.13	0.20	−0.44	15	
	$(^1D)3p\ ^2P^\circ_{3/2}$	52189.8248	233.0	3.5	2.5	2.5	0.3	6	
	$(^1D)3p\ ^2P^\circ_{1/2}$	52424.7882	232	3.6	15	23	−16	4	
$(^3P)3s\ ^2P_{1/2}$	$(^3P)3p\ ^2D^\circ_{3/2}$	26822.8248	209.87	0.50	0.13	0.39	0.21	6	193 (8)
	$(^3P)3p\ ^2S^\circ_{1/2}$	28099.1918	212.95	0.45	0.68	0.93	−1.2	17	
	$(^3P)3p\ ^2P^\circ_{3/2}$	29465.7166	209.91	0.21	0.048	0.20	−0.30	4	221 (6)
	$(^3P)3p\ ^2P^\circ_{1/2}$	29592.8969	211.04	0.10	0.070	0.070	−0.018	7	221 (6)
	$(^1D)3p\ ^2P^\circ_{3/2}$	51577.5611	230.9	3.5	9.6	12	4	5	
	$(^1D)3p\ ^2P^\circ_{1/2}$	51812.5245	230.8	3.6	4.8	7.0	−2.1	6	
$(^1D)3s\ ^2D_{5/2}$	$(^1D)3p\ ^2F^\circ_{5/2}$	27970.4387	158.33	0.48	0.81	1.6	−0.5	13	
	$(^1D)3p\ ^2F^\circ_{7/2}$	28014.9630	158.60	0.37	0.11	0.24		6	162 (16)
	$(^1D)3p\ ^2P^\circ_{3/2}$	29882.7123	155.709	0.082	0.043	0.054	0.036	11	152 (15)
	$(^1D)3p\ ^2D^\circ_{3/2}$	30931.4543	157.5	0.65	1.3	1.3	−4.8	17	
	$(^1D)3p\ ^2D^\circ_{5/2}$	30950.1466	158.14	0.51	0.22	0.34	0.01	12	
	$(^3P)4p\ ^2P^\circ_{3/2}$	47692.3412	194.0	2.5	0.71	1.7	−0.2	3	
$(^1D)3s\ ^2D_{3/2}$	$(^1D)3p\ ^2F^\circ_{5/2}$	27967.0776	158.67	0.33	0.074	0.22	$< 10^{-2}$	11	
	$(^1D)3p\ ^2P^\circ_{3/2}$	29879.3512	156.04	0.34	0.13	0.23	−0.11	17	
	$(^1D)3p\ ^2P^\circ_{1/2}$	30114.3145	155.85	0.11	0.077	0.077	0.024	10	136 (22)
	$(^1D)3p\ ^2D^\circ_{3/2}$	30928.0932	157.92	0.56	0.38	0.38	0.39	11	
	$(^1D)3p\ ^2D^\circ_{5/2}$	30946.7855	158.4	0.61	1.7	1.8	−1.4	14	
	$(^3P)4p\ ^2P^\circ_{3/2}$	47688.9802	194.3	2.6	5.7	5.8	1.4	6	
	$(^3P)4p\ ^2P^\circ_{1/2}$	47935.7087	195.3	2.1	1.1	1.3	−0.1	6	
$(^1S)3s\ ^2S_{1/2}$	$(^1S)3p\ ^2P^\circ_{3/2}$	28721.4814	136.66	0.30	0.19	0.20		10	
	$(^1S)3p\ ^2P^\circ_{1/2}$	28731.3736	137.66	0.67	0.22	0.44		12	
	$(^3P)5p\ ^2P^\circ_{3/2}$	32060.8941	136.6	3.2	1.1	2.1		12	
	$(^3P)5p\ ^2P^\circ_{1/2}$	32299.7183	132.8	4.3	2.2	2.8		15	

[a] Term and level assignment of [21]. [b] Ritz wavenumber of the ^{20}Ne isotope derived in this work. [c] IS and uncertainties derived with error-correction factor $k_1 = 1.51$. [d] One standard deviation uncertainties, given with two significant digits to make the steps in the analysis possible to follow. [e] Uncertainties u_{wm} and u_ϵ of the ordinary and modified weighted means. [f] Number of spectra used to calculate IS_ϵ.

Table 2. Transition isotope shifts in Ne III.

Transition[a]		σ^b	IS^c_{Ritz}	$u^{c,d}_{Ritz}$	$u^{d,e}_{wm}$	$u^{d,e}_{\epsilon}$	$(IS_{Ritz} - IS_{\epsilon})$	spec[f]
Lower	Upper	(cm^{-1})	(10^{-3} cm^{-1})		(10^{-3} cm^{-1})			
$(^4S^\circ)3s\ ^5S^\circ_2$	$(^4S^\circ)3p\ ^5P_1$	38514.474	230.3	4.2	2.5	2.5		10
	$(^4S^\circ)3p\ ^5P_2$	38545.579	233.3	3.8	1.8	2.3		10
	$(^4S^\circ)3p\ ^5P_3$	38598.529	232.2	4.0	1.2	2.4		9
$(^4S^\circ)3s\ ^3S^\circ_1$	$(^4S^\circ)3p\ ^3P_1$	37320.573	393.5	1.4	0.90	0.90		11
	$(^4S^\circ)3p\ ^3P_0$	37330.604	388.2	5.3	2.3	3.2		11
	$(^4S^\circ)3p\ ^3P_2$	37331.532	394.37	0.83	0.50	0.50		10
$(^2D^\circ)3s\ ^3D^\circ_3$	$(^2D^\circ)3p\ ^3D_2$	35921.944	273	10	48	48	−73	1
	$(^2D^\circ)3p\ ^3D_3$	35991.302	281.2	2.7	1.6	1.6	0.1	11
	$(^2D^\circ)3p\ ^3F_3$	38282.093	272.5	8.4	17	17	−11	5
	$(^2D^\circ)3p\ ^3F_4$	38302.647	272.3	1.5	0.92	0.92		12
	$(^2D^\circ)3p\ ^3P_2$	45839.073	257.4	2.7	0.88	1.6	$< 10^{-1}$	10
$(^2D^\circ)3s\ ^3D^\circ_2$	$(^2D^\circ)3p\ ^3D_1$	35881.529	272	11	17	17	−8	5
	$(^2D^\circ)3p\ ^3D_2$	35892.518	275.4	6.7	3.1	4.1	−0.1	10
	$(^2D^\circ)3p\ ^3D_3$	35961.876	283.4	8.4	23	23	−28	3
	$(^2D^\circ)3p\ ^3F_2$	38237.212	259.2	9.2	17	26	−18	4
	$(^2D^\circ)3p\ ^3F_3$	38252.667	274.8	2.6	1.2	1.6	0.1	10
	$(^2D^\circ)3p\ ^3P_2$	45809.646	259.7	7.6	4.9	4.9	−0.4	8
	$(^2D^\circ)3p\ ^3P_1$	45905.660	252.2	3.3	1.7	2.0	0.4	11
$(^2D^\circ)3s\ ^3D^\circ_1$	$(^2D^\circ)3p\ ^3D_1$	35861.396	288.6	8.2	5.2	5.2	0.7	11
	$(^2D^\circ)3p\ ^3D_2$	35872.385	291	10	25	25	22	4
	$(^2D^\circ)3p\ ^3F_2$	38217.078	275.5	3.4	1.8	2.0	0.1	12
	$(^2D^\circ)3p\ ^3P_1$	45885.527	268.5	8.1	4.8	5.3	−2.4	10
	$(^2D^\circ)3p\ ^3P_0$	45928.202	248.4	6.8	4.1	4.1		9
$(^2D^\circ)3s\ ^1D^\circ_2$	$(^2D^\circ)3p\ ^1P_1$	30033.156	374.4	3.1	1.9	1.9		4
	$(^2D^\circ)3p\ ^1F_3$	34872.839	366.6	4.7	2.7	2.8		13
	$(^2D^\circ)3p\ ^1D_2$	48403.427	334.5	2.1	1.2	1.3		9
$(^2P^\circ)3s\ ^3P^\circ_1$	$(^2P^\circ)3p\ ^3D_2$	37885.997	254	18	16	16	27	1
	$(^2P^\circ)3p\ ^3D_1$	37887.009	284	34	29	29	−34	1
	$(^2P^\circ)3p\ ^3P_0$	42233.934	275	26	16	16		3
	$(^2P^\circ)3p\ ^3P_1$	42263.549	261.4	5.4	4.0	4.0	−6.3	11
	$(^2P^\circ)3p\ ^3P_2$	42308.567	263.2	4.6	3.1	3.1	3.3	10
$(^2P^\circ)3s\ ^3P^\circ_0$	$(^2P^\circ)3p\ ^3D_1$	37886.355	278	34	11	29	35	2
	$(^2P^\circ)3p\ ^3P_1$	42262.896	255.9	7.0	3.9	4.2	−0.7	9
$(^2P^\circ)3s\ ^3P^\circ_2$	$(^2P^\circ)3p\ ^3S_1$	35377.255	248	56	34	34		3
	$(^2P^\circ)3p\ ^3D_3$	37851.973	273.2	4.5	2.0	2.7		9
	$(^2P^\circ)3p\ ^3D_2$	37879.435	253	18	15	15	−21	4
	$(^2P^\circ)3p\ ^3P_1$	42256.987	260.2	5.9	3.3	4.9	10	7
	$(^2P^\circ)3p\ ^3P_2$	42302.005	262.0	1.5	0.93	0.93	−0.29	11
$(^2P^\circ)3s\ ^1P^\circ_1$	$(^2D^\circ)3p\ ^1D_2$	26506.051	261	39	23	23		2
	$(^2P^\circ)3p\ ^1P_1$	34402.772	318	33	20	20		6
	$(^2P^\circ)3p\ ^1D_2$	40418.182	311.46	0.63	0.33	0.38		9

[a]Term and level assignment of [22]. [b]Ritz wavenumber of the ^{20}Ne isotope derived in this work. [c]IS and uncertainties derived with error-correction factor $k_1 = 1.65$. [d]One standard deviation uncertainties, given with two significant digits to make the steps in the analysis possible to follow. [e]Uncertainties u_{wm} and u_ϵ of the ordinary and modified weighted means. [f]Number of spectra used to calculate IS_ϵ.

with no observed shifts, the specific mass shifts must be negative, canceling the normal mass shifts.

To see what influence the self-absorption had on the IS, synthetic line profiles were created with the ^{22}Ne/ ^{20}Ne area ratio fixed from the mass spectrometer measurements. The intensity was then modified by one-dimensional radiative-transfer (RT) calculations in a homogeneous plasma,

$$I_{RT}(\sigma) = (1 - e^{-\tau I(\sigma)})/\tau, \qquad (11)$$

where $I(\sigma)$ is the unaffected intensity of the line profile at the wavenumber σ and τ is the product of the optical depth and a factor that normalizes the peak intensity of $I(\sigma)$ to one. From the observed line profiles it was evident that the drop in peak intensity of the ^{20}Ne component never reached more than 10%, which corresponds to an optical depth of about 0.1. With an absorbing plasma of 50 mm in length this gives a mean free path of the emitted photons of 0.5 m for a homogeneous plasma. This is about an order of magnitude larger than the length of the cathode bore, which supports the assumption of a one-dimensional plasma.

Absorption outside the line emitting region, i.e. between the cathode inset and the anode in Figure 1, is not considered explicitly in (11). This absorption is smaller due to the lower population of the 3s level and also the lower abundance of Ne II and Ne III. Its effect is, however, included when modeling the line profiles. From the low optical depths involved and by assuming that the absorption has a spectral distribution close to that within the cathode bore, i.e. no large temperature gradients in the light source, the resulting exponential decay outside the bore can be approximated with an increase of the value of τ.

The resulting synthetic profiles of equation (11) were fitted with the routine with free area ratio between the two isotope components, see Section 4.1 The parameters of the profiles were varied so that the output parameters from the fit covered those from all observed strong transitions. A clear dependence on both Doppler $\delta\sigma_D$ and Lorentzian $\delta\sigma_L$ widths was found, see Figure 4.

All observed strong transitions involving 3s ^{2}P levels can be reproduced with optical depths corresponding to a 5–10% peak intensity reduction of the ^{20}Ne component. In low current spectra, they all have a $\delta\sigma_D/IS$ below 0.50, which gives systematic red shifts up to 0.0003 cm^{-1} from the true value. For the transitions with a 3s ^{2}D lower level, the corresponding intensity reduction and ratio is 3–5% and 0.65, respectively, giving a blue shift below 0.0006 cm^{-1}. All other transitions can be reproduced with the same reduction but a ratio below 0.75, which gives a 0.001 cm^{-1} limit to the blue shift.

Another source of error is the ^{21}Ne isotope and to estimate an upper limit to its influence another set of synthetic line profiles was generated. The center of gravity of the ^{21}Ne hfs-profile was determined by equation (1) and the total area of the profile was fixed by the ratio from the mass spectrometer measurements. Profiles were generated with $\delta\sigma_D/IS$ of 0.50 and 0.75 and the change in IS from the true value was derived as a function of distance $\delta\sigma_{hfs}$ between the outermost hfs-components, see Figure 5. From the residuals of the observed data, it is clear that all strong transitions have a $\delta\sigma_{hfs}/IS$ above 0.5. A ^{21}Ne profile with only two hfs-components will have the largest impact, since more components can have a canceling effect. This two-component worst-case scenario can give a deviation from the true value in the range $(-5$ to $9)\times10^{-4}$ cm^{-1}. However, an error of $(-5$ to $5)\times10^{-4}$ cm^{-1} from a four-component hfs is more likely.

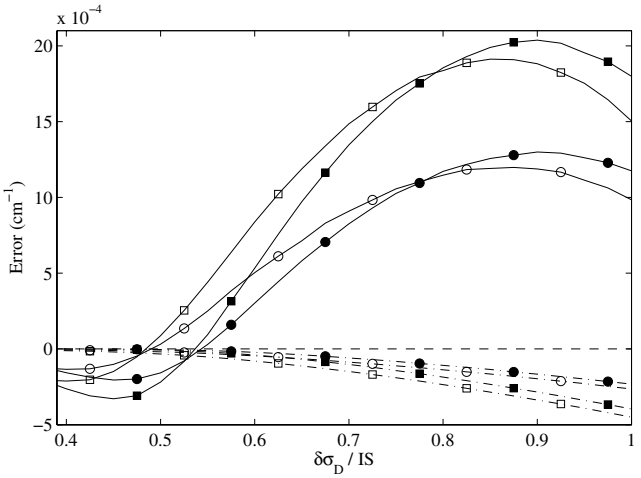

Fig. 4. Shift from true value of isotope shift IS caused by self-absorption (solid line), plotted as a function of the Doppler width $\delta\sigma_D$ over IS ratio. The two sets of data correspond to a ^{20}Ne peak intensity loss of 5% (circles) and 10% (squares), where the latter has the larger error amplitude. Filled symbols correspond to a Lorentzian width $\delta\sigma_L$ of 0.002 cm^{-1} and empty 0.02 cm^{-1}. Errors in absolute position of ^{20}Ne decrease monotonically and are shown in the lower set of curves (dashed-dotted lines).

Depending on the parameters of an observed profile, the errors introduced from self-absorption and ^{21}Ne may add or subtract. If the latter is the case, the total error can be severely overestimated. Due to this, and that the estimated errors are conservative, they were not regarded in the analysis. Instead, to minimize the errors, when calculating the mean (8) of all strong transitions, only low current spectra were used ($I < 0.4$ A), where both effects discussed above have a smaller impact. For many of the stronger Ne II transitions the weighted means still had χ^2_ϵ that were too large to be explained by statistical variations. Instead, this is a combined effect of the systematic errors described above and the correlated noise discussed in Section 4.4. A non-zero ϵ had to be introduced, resulting in $u_\epsilon > u_{wm}$ in Table 1 for these Ne II transitions. The weaker transitions, including all Ne III, had reduced χ^2_ϵ with small deviations from unity. This can be explained by the much lower S/N of the lines, which renders the systematic errors insignificant.

To test for systematic errors in the results, the derived IS means were added to the Ritz wavenumbers σ_{Ritz} of ^{20}Ne, see Section 5.3, followed by a fit to the energy levels involved using the method described in Section 4.2. Only the uncertainties of the shifts were considered, since the

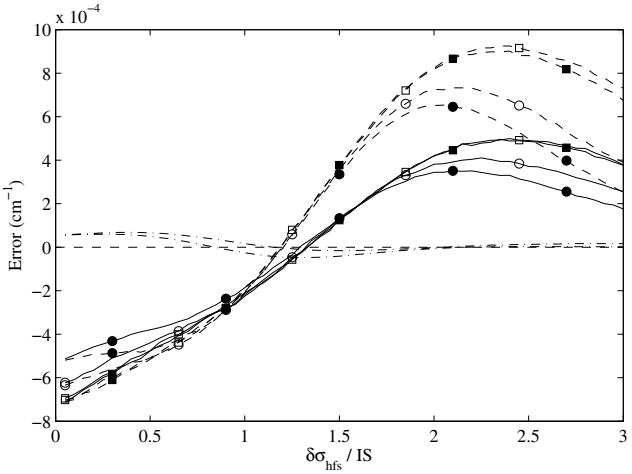

Fig. 5. Shift from true value of isotope shift IS introduced by omitting ^{21}Ne, plotted as a function of the ratio formed by the distance $\delta\sigma_{hfs}$ between the two outermost hfs-components in ^{21}Ne over the IS. The two sets of data correspond to an unsplitted $J = 3/2$ upper level and a $J = 1/2$ (dashed) and 3/2 (solid) lower level, respectively, where the latter has the smallest amplitude. Errors for $\delta\sigma_D/IS$ of 0.50 (circles) and 0.75 (squares) are shown. Filled symbols correspond to a Lorentzian width $\delta\sigma_L$ of 0.002 cm^{-1} and empty 0.02 cm^{-1}. Amplitudes increase both with Doppler and Lorentzian widths. Typical errors in absolute position of ^{20}Ne are also shown (dashed-dotted lines).

σ_{Ritz}, being a unique solution of the level system, were used only to define what levels are involved. The influence of the Stark effect on the energy of a level was assumed to be the same for the two isotopes, making its effect on the IS negligible. The uncertainties needed to be modified with a k_1 of 1.51 and 1.65 for Ne II and Ne III, respectively, in (3), while k_2 had no influence on χ^2 and was set to zero. After fitting, the σ_{Ritz} were subtracted to yield the final isotope shifts IS_{Ritz}, which are presented in Tables 1 and 2. In this way the IS of all transitions defining energy levels in a closed loop are correlated.

Clearly, from the values of k_1 and the discussion in Section 4.4, the correlated noise had been compensated for. All IS_{Ritz} fell within two u_ϵ from corresponding value of IS_ϵ, see Tables 1 and 2, showing a strong internal consistency of the observed data. However, the accuracy of the IS_{Ritz} may be overestimated for those transitions that have uncertainties u_{Ritz} that are lower than the estimated errors from self-absorption and the omitted ^{21}Ne isotope.

Synthetic line profiles, with typical experimental parameters, were also studied to determine when the IS can be resolved. The sum of the two isotope components was fitted with a pure Voigt function. From the residual, evaluated both by eye and the reduced χ^2, an upper conservative limit of the IS was found as a function of $\delta\lambda_D$ and the S/N of the Voigt. For lines with S/N less than 30 the ^{22}Ne component is too weak to set a limit without any prior knowledge of the shift. The limiting intervals for the 3p–3d and 3p–4s IS are given in Tables 3 and 4.

5.2 Absolute line position of ^{20}Ne

Accurate argon wavenumbers have been measured by Whaling et al. [7], using high-resolution FTS spectra from a DC HC. They recommend a number of strong 3d–4p and 4s–4p transitions in Ar II as secondary standards, those being the least sensitive to Stark shifts. The wavenumbers are stated with an accuracy of 0.0002 to 0.0003 cm^{-1}, given as conservative estimates with the true uncertainties even lower. In this work, these transitions are used to calibrate the neon spectra in the spectral region **A**. There are no Ar II standards available in region **B**. Instead, Ne II transitions present in the overlap of the regions were used. To make these calibrations as accurate as possible, a thorough analysis of all neon lines of region **A** was first performed, including the steps described in Sections 4.1–4.3.

In a FTS spectrum the observed wavenumber σ_{obs} has to be corrected by

$$\sigma_{corr} = (1 + \alpha)\sigma_{obs}, \tag{12}$$

where α is a constant [24]. For each reference line, a value of α was calculated with uncertainties derived by error propagation, taking both the uncertainty of the reference wavenumber and the fitting into account. About 20 Ar II transitions were used in each region **A** spectrum and a mean of α was then calculated using (8). In low current spectra, the reduced χ^2_ϵ were close to unity, see Table 7. For high currents, χ^2_ϵ were far too large for statistical variations. The main contribution to this effect came from a handful Ar II transitions, deviating in both directions from the bulk of the lines. Assuming large Stark shifts or unidentified blends being responsible, these lines were removed from the mean. By error propagation, $u_\epsilon(\alpha)$ was then added to the uncertainty of the measured neon lines. When transferring the calibration to region **B** as described above, α showed a current dependence that was smaller than for Ar II in region **A**.

As for the IS in Section 5.1, self-absorption and the omitted ^{21}Ne isotope will affect the absolute position of the ^{20}Ne component for strong 3s–3p transitions. Synthetic line profiles were studied to get a conservative estimate of the errors. Self-absorption will cause a red shift from the true value that is roughly linear with $\delta\sigma_D/IS$, see Figure 4. Lines in low-current spectra with 3s ^{2}P or 3s ^{2}D lower levels will shift less than 2×10^{-5} cm^{-1}, while the largest shifts for all other transitions are 6×10^{-5} cm^{-1}. The ^{21}Ne isotope will introduce errors behaving as those for the IS, see Figure 5, but the amplitude is an order of magnitude lower. For the two-component scenario the error is covered by $(-6$ to $6) \times 10^{-5}$ cm^{-1}, while the more probable four-component error is in the range $(-2$ to $6) \times 10^{-5}$ cm^{-1}. The error amplitudes from these two sources increase with both Doppler and Lorentzian widths, motivating the use of low-current spectra. Another reason for using these spectra are Stark shifts, which have a larger impact on the absolute positions, see Section 6.

After fitting the spectral lines, modified means (8) of the line center positions of ^{20}Ne were calculated. If a spectral line made a big contribution to χ^2_ϵ and a Stark shift or

Table 3. Finding list for observed Ne II 3s–np, 3p–3d, 3p–4s transitions.

σ^a_{Ritz} (cm^{-1})	$u^{a,b}_{Ritz}$	u^b_{wm} (10^{-3} cm^{-1})	u^b_ϵ (10^{-3} cm^{-1})	$\sigma_{Ritz}-\sigma_\epsilon$	spec[c]	S/N^d (log)	IS^e (10^{-3})	Transition Lower	Transition Upper	λ^f (Å)
22512.1285	4.8	2.8	3.1	$< 10^{-1}$	7	0.7		$(^3P)3p\ ^2P^\circ_{3/2}$	$(^1S)3s\ ^2S_{1/2}$	4440.8032
24996.23285	0.14	4.3	5.5	0.7	4	0.6		$(^3P)3s\ ^2P_{1/2}$	$(^3P)3p\ ^4D^\circ_{3/2}$	3999.4720
25358.95447	0.12	1.9	2.1	−0.4	1	1.1	209	$(^3P)3s\ ^2P_{3/2}$	$(^3P)3p\ ^4D^\circ_{5/2}$	3942.2643
26103.95702	0.13	0.059	0.11	0.04	12	2.4	< 61	$(^3P)3p\ ^2P^\circ_{3/2}$	$(^3P)3d\ ^2D_{5/2}$	3829.7502
26181.38831	0.16	0.12	0.14	0.07	16	2.1	< 73	$(^3P)3p\ ^2P^\circ_{1/2}$	$(^3P)3d\ ^2D_{3/2}$	3818.4235
26265.12497	0.18	2.8	2.8	−7.0	7	0.9		$(^3P)3p\ ^4S^\circ_{3/2}$	$(^3P)3d\ ^4D_{5/2}$	3806.2495
26308.56861	0.17	0.21	0.25	0.33	15	2.0	< 80	$(^3P)3p\ ^2P^\circ_{3/2}$	$(^3P)3d\ ^2D_{3/2}$	3799.9641
26371.35658	0.21	3.0	4.8	−2.3	7	0.9		$(^3P)3p\ ^4S^\circ_{3/2}$	$(^3P)3d\ ^4D_{3/2}$	3790.9165
26467.568116	0.092	0.029	0.029	−0.14	11	2.9	130	$(^3P)3s\ ^4P_{1/2}$	$(^3P)3p\ ^4P^\circ_{3/2}$	3777.1359
26543.985930	0.089	0.025	0.025	−0.054	16	2.9	130	$(^3P)3s\ ^4P_{3/2}$	$(^3P)3p\ ^4P^\circ_{5/2}$	3766.2616
26624.40646	0.33	13	13	20	1	0.6		$(^3P)3p\ ^2S^\circ_{1/2}$	$(^3P)3d\ ^4D_{1/2}$	3754.8851
26632.25145	0.14	0.11	0.11	0.10	16	2.3	< 68	$(^3P)3p\ ^2P^\circ_{3/2}$	$(^3P)3d\ ^4F_{5/2}$	3753.7790
26650.23526	0.10	0.074	0.074	−0.12	16	2.3	130	$(^3P)3s\ ^4P_{1/2}$	$(^3P)3p\ ^4P^\circ_{1/2}$	3751.2458
26654.90854	0.19	9.5	23	27	2	0.5		$(^3P)3p\ ^2P^\circ_{1/2}$	$(^3P)3d\ ^4F_{3/2}$	3750.5881
26697.35434	0.20	0.36	0.46	0.12	15	1.9	< 110	$(^3P)3p\ ^2P^\circ_{1/2}$	$(^3P)3d\ ^4P_{3/2}$	3744.6250
26766.586961	0.086	0.052	0.052	−0.27	12	2.5	131	$(^3P)3s\ ^4P_{3/2}$	$(^3P)3p\ ^4P^\circ_{3/2}$	3734.9391
26782.08884	0.18	30	30	6	1	0.4		$(^3P)3p\ ^2P^\circ_{3/2}$	$(^3P)3d\ ^4F_{3/2}$	3732.7772
26822.824832	0.090	0.036	0.036	0.094	7	3.0	210	$(^3P)3s\ ^2P_{1/2}$	$(^3P)3p\ ^2D^\circ_{3/2}$	3727.1081
26824.53464	0.20	0.79	0.79	0.23	13	1.5	< 265	$(^3P)3p\ ^2P^\circ_{3/2}$	$(^3P)3d\ ^4P_{3/2}$	3726.8705
26860.94598	0.14	0.42	0.45	0.32	15	1.8	< 121	$(^3P)3p\ ^2P^\circ_{3/2}$	$(^3P)3d\ ^2F_{5/2}$	3721.8184
26924.142614	0.098	0.040	0.040	−0.19	4	2.9	210	$(^3P)3s\ ^2P_{3/2}$	$(^3P)3p\ ^2D^\circ_{5/2}$	3713.0823
26949.254114	0.095	0.021	0.021	0.088	12	3.0	132	$(^3P)3s\ ^4P_{3/2}$	$(^3P)3p\ ^4P^\circ_{1/2}$	3709.6224
27006.36878	0.12	0.12	0.12	−0.19	18	2.4	< 62	$(^3P)3p\ ^2P^\circ_{3/2}$	$(^3P)3d\ ^4P_{5/2}$	3701.7768
27040.35288	0.30	0.71	0.92	−1.8	13	1.6	< 165	$(^3P)3p\ ^2P^\circ_{1/2}$	$(^3P)3d\ ^2P_{1/2}$	3697.1244
27061.650312	0.086	0.027	0.027	0.070	10	3.4	131	$(^3P)3s\ ^4P_{5/2}$	$(^3P)3p\ ^4P^\circ_{5/2}$	3694.2147
27167.53317	0.30	0.52	0.85	−1.2	13	1.7	< 130	$(^3P)3p\ ^2P^\circ_{3/2}$	$(^3P)3d\ ^2P_{1/2}$	3679.8164
27284.251343	0.088	0.024	0.024	−0.10	10	3.0	132	$(^3P)3s\ ^4P_{5/2}$	$(^3P)3p\ ^4P^\circ_{3/2}$	3664.0743
27315.42734	0.16	0.54	0.67	−0.79	16	1.7	< 146	$(^3P)3p\ ^4S^\circ_{3/2}$	$(^3P)3d\ ^2D_{5/2}$	3659.8923
27428.10606	0.12	0.083	0.085	0.006	15	2.6	< 67	$(^3P)3p\ ^2P^\circ_{1/2}$	$(^3P)3d\ ^2P_{3/2}$	3644.8565
27435.088543	0.088	0.028	0.041	−0.061	10	2.9	212	$(^3P)3s\ ^2P_{3/2}$	$(^3P)3p\ ^2D^\circ_{3/2}$	3643.9288
27520.03892	0.20	0.70	0.70	0.04	5	1.7	< 143	$(^3P)3p\ ^4S^\circ_{3/2}$	$(^3P)3d\ ^2D_{3/2}$	3632.6802
27555.28636	0.13	0.16	0.16	0.19	16	2.3	< 91	$(^3P)3p\ ^2P^\circ_{3/2}$	$(^3P)3d\ ^2P_{3/2}$	3628.0333
27675.09337	0.18	0.42	0.53	0.10	11	1.5	< 105	$(^3P)3p\ ^2S^\circ_{1/2}$	$(^3P)3d\ ^2D_{3/2}$	3612.3270
27814.99022	0.22	0.13	0.13	−0.04	15	2.0	< 58	$(^3P)3p\ ^4S^\circ_{3/2}$	$(^3P)3d\ ^4P_{1/2}$	3594.1581
27833.27756	0.21	2.9	5.1	−12	6	1.1		$(^3P)3p\ ^2P^\circ_{3/2}$	$(^3P)4s\ ^4P_{5/2}$	3591.7966
27843.72177	0.15	1.0	1.0	1.0	13	1.5	< 144	$(^3P)3p\ ^4S^\circ_{3/2}$	$(^3P)3d\ ^4F_{5/2}$	3590.4492
27967.077589	0.099	0.013	0.020	−0.007	11	3.4	159	$(^1D)3s\ ^2D_{3/2}$	$(^1D)3p\ ^2F^\circ_{5/2}$	3574.6122
27970.43866	0.12	0.078	0.11	−0.10	13	2.3	158	$(^1D)3s\ ^2D_{5/2}$	$(^1D)3p\ ^2F^\circ_{5/2}$	3574.1827
27993.55915	0.15	0.11	0.11	0.09	11	2.2	< 55	$(^3P)3p\ ^4S^\circ_{3/2}$	$(^3P)3d\ ^4F_{3/2}$	3571.2306
28014.96302	0.10	0.033	0.033	0.056	6	3.2	159	$(^1D)3s\ ^2D_{5/2}$	$(^1D)3p\ ^2F^\circ_{7/2}$	3568.5020
28036.00496	0.18	0.14	0.19	0.03	15	2.0	< 63	$(^3P)3p\ ^4S^\circ_{3/2}$	$(^3P)3d\ ^4P_{3/2}$	3565.8237
28072.41629	0.15	0.09.	0.14	0.10	12	2.6	< 59	$(^3P)3p\ ^4S^\circ_{3/2}$	$(^3P)3d\ ^2F_{5/2}$	3561.1985
28083.13801	0.20	2.2	2.2	5.1	8	1.1		$(^3P)3p\ ^2P^\circ_{1/2}$	$(^3P)4s\ ^4P_{3/2}$	3559.8388
28099.19180	0.10	0.069	0.069	0.15	19	2.6	213	$(^3P)3s\ ^2P_{1/2}$	$(^3P)3p\ ^2S^\circ_{1/2}$	3557.8050
28126.45530[g]	0.17	4.4	4.4	−9.3	4	0.9		$(^3P)3p\ ^2D^\circ_{5/2}$	$(^3P)3d\ ^4D_{7/2}$	3554.3562
28148.61360	0.20	3.9	3.9	0.6	5	1.0		$(^3P)3p\ ^2S^\circ_{1/2}$	$(^3P)3d\ ^4F_{3/2}$	3551.5582
28191.05940	0.21	1.3	1.4	−2.8	11	1.4		$(^3P)3p\ ^2S^\circ_{1/2}$	$(^3P)3d\ ^4P_{3/2}$	3546.2106
28210.31831	0.19	0.68	0.68	0.89	13	1.7	< 87	$(^3P)3p\ ^2P^\circ_{3/2}$	$(^3P)4s\ ^4P_{3/2}$	3543.7896
28217.83910	0.12	0.048	0.063	−0.29	13	2.5	< 68	$(^3P)3p\ ^4S^\circ_{3/2}$	$(^3P)3d\ ^4P_{5/2}$	3542.8451
28222.65430	0.27	0.26	0.26	0.43	13	2.1	< 109	$(^1D)3p\ ^2D^\circ_{5/2}$	$(^1D)3d\ ^2P_{3/2}$	3542.2406
28241.34657	0.29	6.1	6.1	6.0	4	0.7		$(^1D)3p\ ^2D^\circ_{3/2}$	$(^1D)3d\ ^2P_{3/2}$	3539.8960
28256.67366	0.40	0.41	0.41	0.63	17	1.8	< 133	$(^1D)3p\ ^2D^\circ_{3/2}$	$(^1D)3d\ ^2P_{1/2}$	3537.9758
28379.00349	0.32	5.0	5.5	−3.6	4	0.8		$(^3P)3p\ ^4S^\circ_{3/2}$	$(^3P)3d\ ^2P_{1/2}$	3522.7247
28534.05794	0.29	0.18	0.18	−0.01	2	2.1	< 77	$(^3P)3p\ ^2S^\circ_{1/2}$	$(^3P)3d\ ^2P_{1/2}$	3503.5816

Table 3. *Continued.*

σ^a_{Ritz} (cm^{-1})	$u^{a,b}_{Ritz}$	u^b_{wm} (10^{-3} cm^{-1})	u^b_ϵ (10^{-3} cm^{-1})	$\sigma_{Ritz}-\sigma_\epsilon$	spec[c]	S/N^d (log)	IS^e (10^{-3})	Transition Lower	Transition Upper	λ^f (Å)
28711.455512	0.096	0.024	0.042	0.065	10	2.9	215	$(^3P)3s\ ^2P_{3/2}$	$(^3P)3p\ ^2S^\circ_{1/2}$	3481.9336
28721.48143	0.14	0.024	0.056	0.019	8	3.1	137	$(^1S)3s\ ^2S_{1/2}$	$(^1S)3p\ ^2P^\circ_{3/2}$	3480.7181
28731.37355	0.12	0.036	0.036	−0.002	10	2.8	138	$(^1S)3s\ ^2S_{1/2}$	$(^1S)3p\ ^2P^\circ_{1/2}$	3479.5197
28746.84875	0.15	0.22	0.34	−0.46	14	1.9	< 104	$(^3P)3p\ ^2D^\circ_{3/2}$	$(^3P)3d\ ^2D_{5/2}$	3477.6465
28766.75668	0.17	5.7	5.7	5.8	4	0.8		$(^3P)3p\ ^4S^\circ_{3/2}$	$(^3P)3d\ ^2P_{3/2}$	3475.2397
28899.14048	0.14	0.063	0.063	0.080	12	2.4	< 71	$(^1D)3p\ ^2D^\circ_{5/2}$	$(^1D)3d\ ^2D_{5/2}$	3459.3196
28917.83276	0.20	0.71	0.71	1.2	14	1.6	< 174	$(^1D)3p\ ^2D^\circ_{3/2}$	$(^1D)3d\ ^2D_{5/2}$	3457.0834
28918.48663	0.22	0.79	1.1	−3.1	14	1.6	< 181	$(^1D)3p\ ^2D^\circ_{5/2}$	$(^1D)3d\ ^2D_{3/2}$	3457.0053
28921.81112	0.12	0.086	0.086	0.14	14	2.3	< 73	$(^3P)3p\ ^2S^\circ_{1/2}$	$(^3P)3d\ ^2P_{3/2}$	3456.6079
28937.17891	0.16	0.080	0.085	−0.11	15	2.6	< 80	$(^1D)3p\ ^2D^\circ_{3/2}$	$(^1D)3d\ ^2D_{3/2}$	3454.7721
28951.46034	0.17	0.18	0.18	−0.33	18	2.2	< 93	$(^3P)3p\ ^2D^\circ_{3/2}$	$(^3P)3d\ ^2D_{3/2}$	3453.0679
29030.16237	0.13	0.29	0.29	0.31	15	2.0	< 104	$(^3P)3p\ ^2P^\circ_{1/2}$	$(^3P)4s\ ^2P_{3/2}$	3443.7062
29044.74788	0.20	1.2	1.2	0.01	13	1.4	< 200	$(^3P)3p\ ^4S^\circ_{3/2}$	$(^3P)4s\ ^4P_{5/2}$	3441.9768
29055.12525	0.28	0.68	0.68	−0.32	14	1.6	< 199	$(^1D)3p\ ^2P^\circ_{1/2}$	$(^1D)3d\ ^2P_{3/2}$	3440.7474
29070.45233	0.40	0.34	0.37	−0.24	16	1.9	< 132	$(^1D)3p\ ^2P^\circ_{1/2}$	$(^1D)3d\ ^2P_{1/2}$	3438.9332
29157.34267	0.11	0.062	0.071	0.090	12	2.4	< 70	$(^3P)3p\ ^2P^\circ_{3/2}$	$(^3P)4s\ ^2P_{3/2}$	3428.6847
29251.16612	0.10	0.031	0.031	−0.084	15	3.1	< 65	$(^3P)3p\ ^2D^\circ_{5/2}$	$(^3P)3d\ ^2F_{7/2}$	3417.6868
29257.79468	0.13	0.095	0.10	0.04	14	2.5	< 75	$(^3P)3p\ ^2D^\circ_{5/2}$	$(^3P)3d\ ^2D_{5/2}$	3416.9125
29275.14319	0.15	0.82	0.82	2.2	13	1.3		$(^3P)3p\ ^2D^\circ_{3/2}$	$(^3P)3d\ ^4F_{5/2}$	3414.8876
29290.08859	0.26	0.22	0.22	−0.23	3	2.0	< 88	$(^1D)3p\ ^2P^\circ_{3/2}$	$(^1D)3d\ ^2P_{3/2}$	3413.1451
29305.41568	0.41	0.65	0.65	−1.5	14	1.6	< 187	$(^1D)3p\ ^2P^\circ_{3/2}$	$(^1D)3d\ ^2P_{1/2}$	3411.3599
29343.00566[g]	0.24	1.8	1.8	6.1	5	1.0		$(^1D)3p\ ^2D^\circ_{5/2}$	$(^1D)3d\ ^2F_{5/2}$	3406.9896
29343.39109	0.13	0.052	0.053	0.11	16	2.7	< 66	$(^1D)3p\ ^2D^\circ_{5/2}$	$(^1D)3d\ ^2F_{7/2}$	3406.9449
29361.69794	0.19	0.086	0.10	0.08	14	2.3	< 67	$(^1D)3p\ ^2D^\circ_{3/2}$	$(^1D)3d\ ^2F_{5/2}$	3404.8206
29421.78862	0.19	2.0	2.0	0.28	10	1.0		$(^3P)3p\ ^4S^\circ_{3/2}$	$(^3P)4s\ ^4P_{3/2}$	3397.8664
29462.40627	0.18	0.91	0.91	0.76	16	1.5	< 183	$(^3P)3p\ ^2D^\circ_{5/2}$	$(^3P)3d\ ^2D_{3/2}$	3393.1819
29465.716566	0.088	0.018	0.037	−0.035	8	3.5	210	$(^3P)3s\ ^2P_{1/2}$	$(^3P)3p\ ^2P^\circ_{3/2}$	3392.8007
29467.42637	0.20	0.64	1.3	−1.9	11	1.7	< 219	$(^3P)3p\ ^2D^\circ_{3/2}$	$(^3P)3d\ ^4P_{3/2}$	3392.6038
29485.25712	0.22	1.1	1.3	−0.03	12	1.4		$(^3P)3p\ ^4D^\circ_{1/2}$	$(^3P)3d\ ^4D_{3/2}$	3390.5521
29499.25885	0.17	0.15	0.16	−0.27	17	2.2	< 103	$(^1D)3p\ ^2P^\circ_{1/2}$	$(^1D)3d\ ^2S_{1/2}$	3388.9427
29503.83771	0.12	0.052	0.055	0.088	11	2.6	< 71	$(^3P)3p\ ^2D^\circ_{3/2}$	$(^3P)3d\ ^2F_{5/2}$	3388.4168
29523.13836	0.17	1.0	1.0	0.4	13	1.4	< 135	$(^3P)3p\ ^4D^\circ_{3/2}$	$(^3P)3d\ ^4D_{5/2}$	3386.2015
29583.25254	0.32	0.66	0.66	0.17	16	1.6	< 196	$(^3P)3p\ ^4D^\circ_{1/2}$	$(^3P)3d\ ^4D_{1/2}$	3379.3204
29592.896864	0.088	0.029	0.029	0.050	7	3.4	211	$(^3P)3s\ ^2P_{1/2}$	$(^3P)3p\ ^2P^\circ_{1/2}$	3378.2191
29602.22729	0.13	0.097	0.097	0.17	13	2.2	< 75	$(^3P)3p\ ^2P^\circ_{1/2}$	$(^3P)4s\ ^2P_{1/2}$	3377.1543
29629.36998	0.20	0.38	0.38	0.52	14	1.7	< 78	$(^3P)3p\ ^4D^\circ_{3/2}$	$(^3P)3d\ ^4D_{3/2}$	3374.0604
29649.26051	0.12	0.10	0.10	0.16	17	2.4	< 59	$(^3P)3p\ ^2D^\circ_{3/2}$	$(^3P)3d\ ^4P_{5/2}$	3371.7968
29689.59494	0.10	0.036	0.036	0.15	14	3.0	< 63	$(^3P)3p\ ^2D^\circ_{5/2}$	$(^3P)3d\ ^4F_{7/2}$	3367.2160
29691.64344	0.14	1.8	1.8	0.3	9	1.2		$(^3P)3p\ ^4D^\circ_{5/2}$	$(^3P)3d\ ^4D_{7/2}$	3366.9837
29727.11219[g]	0.27	1.7	2.2	1.3	6	1.5	< 312	$(^3P)3p\ ^4S^\circ_{3/2}$	$(^3P)4s\ ^4P_{1/2}$	3362.9662
29727.36540	0.31	0.62	0.86	0.21	12	1.8	< 119	$(^3P)3p\ ^4D^\circ_{3/2}$	$(^3P)3d\ ^4D_{1/2}$	3362.9376
29729.40759	0.14	0.16	0.17	0.16	17	2.0	< 89	$(^3P)3p\ ^2P^\circ_{3/2}$	$(^3P)4s\ ^2P_{1/2}$	3362.7066
29734.22219	0.15	0.086	0.086	0.23	15	2.5	< 84	$(^1D)3p\ ^2P^\circ_{3/2}$	$(^1D)3d\ ^2S_{1/2}$	3362.1621
29748.059396	0.096	0.042	0.045	−0.13	11	2.8	125	$(^3P)3s\ ^4P_{1/2}$	$(^3P)3p\ ^4D^\circ_{3/2}$	3360.5981
29750.95758	0.21	0.36	0.36	0.81	16	1.9	< 126	$(^1D)3p\ ^2P^\circ_{1/2}$	$(^1D)3d\ ^2D_{3/2}$	3360.2707
29772.68045	0.16	0.16	0.21	−0.05	15	2.0	< 50	$(^3P)3p\ ^4D^\circ_{5/2}$	$(^3P)3d\ ^4D_{5/2}$	3357.8189
29786.08911	0.15	0.54	0.67	1.0	12	1.7	< 130	$(^3P)3p\ ^2D^\circ_{5/2}$	$(^3P)3d\ ^4F_{5/2}$	3356.3073
29797.536150	0.090	0.023	0.038	−0.16	11	3.2	126	$(^3P)3s\ ^4P_{3/2}$	$(^3P)3p\ ^4D^\circ_{5/2}$	3355.0179
29810.42491	0.31	1.0	1.0	0.5	13	1.4		$(^3P)3p\ ^2D^\circ_{3/2}$	$(^3P)3d\ ^2P_{1/2}$	3353.5673
29878.91207[g]	0.20	0.91	0.91	−1.2	2	1.5	< 193	$(^3P)3p\ ^4D^\circ_{5/2}$	$(^3P)3d\ ^4D_{3/2}$	3345.8801
29879.351196	0.096	0.027	0.027	−0.13	8	3.1	156	$(^1D)3s\ ^2D_{3/2}$	$(^1D)3p\ ^2P^\circ_{3/2}$	3345.8310
29882.712268	0.095	0.036	0.036	−0.16	5	3.3	155	$(^1D)3s\ ^2D_{5/2}$	$(^1D)3p\ ^2P^\circ_{3/2}$	3345.4546
29892.17225	0.11	0.043	0.043	−0.16	11	2.8	124	$(^3P)3s\ ^4P_{1/2}$	$(^3P)3p\ ^4D^\circ_{1/2}$	3344.3959
29966.57478	0.17	0.17	0.24	0.01	16	2.1	< 96	$(^1D)3p\ ^2P^\circ_{3/2}$	$(^1D)3d\ ^2D_{5/2}$	3336.0919

Table 3. *Continued.*

σ^a_{Ritz} (cm^{-1})	$u^{a,b}_{Ritz}$	u^b_{wm} (10^{-3} cm^{-1})	u^b_ϵ (10^{-3} cm^{-1})	$\sigma_{Ritz}-\sigma_\epsilon$	spec[c]	S/N^d (log)	IS^e (10^{-3})	Transition Lower	Transition Upper	λ^f (Å)
29977.851725	0.099	0.021	0.021	−0.14	10	3.2	126	$(^3P)3s\ ^4P_{5/2}$	$(^3P)3p\ ^4D^\circ_{7/2}$	3334.8369
29985.92093[g]	0.20	3.4	3.4	5.7	5	0.9		$(^1D)3p\ ^2P^\circ_{3/2}$	$(^1D)3d\ ^2D_{3/2}$	3333.9395
30014.78364	0.15	0.68	0.68	1.0	11	1.6	< 145	$(^3P)3p\ ^2D^\circ_{5/2}$	$(^3P)3d\ ^2F_{5/2}$	3330.7334
30028.99225	0.12	0.070	0.073	−0.27	17	2.6	< 044	$(^3P)3p\ ^4D^\circ_{7/2}$	$(^3P)3d\ ^4D_{7/2}$	3329.1574
30047.078242	0.092	0.041	0.041	−0.038	10	2.8	127	$(^3P)3s\ ^4P_{3/2}$	$(^3P)3p\ ^4D^\circ_{3/2}$	3327.1534
30077.980276	0.082	0.034	0.034	−0.20	5	3.5	212	$(^3P)3s\ ^2P_{3/2}$	$(^3P)3p\ ^2P^\circ_{3/2}$	3323.7350
30110.02926	0.17	0.29	0.29	−0.33	18	2.0	< 78	$(^3P)3p\ ^4D^\circ_{7/2}$	$(^3P)3d\ ^4D_{5/2}$	3320.1971
30114.31454	0.10	0.018	0.018	−0.056	7	3.4	156	$(^1D)3s\ ^2D_{3/2}$	$(^1D)3p\ ^2P^\circ_{1/2}$	3319.7247
30160.20644	0.14	2.4	2.4	−1.5	7	1.0		$(^3P)3p\ ^2D^\circ_{5/2}$	$(^3P)3d\ ^4P_{5/2}$	3314.6732
30191.19110	0.12	0.22	0.22	−0.11	3	1.9	126	$(^3P)3s\ ^4P_{3/2}$	$(^3P)3p\ ^4D^\circ_{1/2}$	3311.2713
30198.17809	0.14	1.1	1.2	−1.6	13	1.3		$(^3P)3p\ ^2D^\circ_{3/2}$	$(^3P)3d\ ^2P_{3/2}$	3310.5051
30205.160574	0.086	0.026	0.026	−0.10	9	3.3	213	$(^3P)3s\ ^2P_{3/2}$	$(^3P)3p\ ^2P^\circ_{1/2}$	3309.7398
30315.200532	0.096	0.052	0.057	−0.14	11	2.6	127	$(^3P)3s\ ^4P_{5/2}$	$(^3P)3p\ ^4D^\circ_{5/2}$	3297.7255
30523.86743	0.14	0.23	0.23	0.35	15	2.0	< 111	$(^3P)3p\ ^2S^\circ_{1/2}$	$(^3P)4s\ ^2P_{3/2}$	3275.1809
30564.74262	0.11	0.30	0.41	0.62	15	1.9	128	$(^3P)3s\ ^4P_{5/2}$	$(^3P)3p\ ^4D^\circ_{3/2}$	3270.8007
30573.44073	0.16	0.23	0.23	−0.11	17	2.0	< 116	$(^3P)3p\ ^4D^\circ_{3/2}$	$(^3P)3d\ ^2D_{5/2}$	3269.8702
30633.93946	0.22	0.60	0.61	−0.80	14	1.4	< 161	$(^3P)3p\ ^4D^\circ_{1/2}$	$(^3P)3d\ ^2D_{3/2}$	3263.4123
30709.12402	0.15	0.94	1.0	1.1	14	1.4		$(^3P)3p\ ^2D^\circ_{5/2}$	$(^3P)3d\ ^2P_{3/2}$	3255.4223
30756.97934	0.13	0.11	0.12	0.08	17	2.2	< 86	$(^1D)3p\ ^2D^\circ_{5/2}$	$(^1D)4s\ ^2D_{5/2}$	3250.3569
30757.33851[g]	0.18	1.6	1.6	0.48	7	1.1		$(^1D)3p\ ^2D^\circ_{5/2}$	$(^1D)4s\ ^2D_{3/2}$	3250.3190
30775.67162[g]	0.17	1.0	1.0	$< 10^{-1}$	7	1.3		$(^1D)3p\ ^2D^\circ_{3/2}$	$(^1D)4s\ ^2D_{5/2}$	3248.3827
30776.03079	0.16	0.20	0.20	−0.15	13	2.0	< 109	$(^1D)3p\ ^2D^\circ_{3/2}$	$(^1D)4s\ ^2D_{3/2}$	3248.3448
30778.05232	0.20	0.73	0.73	−0.04	15	1.5	< 218	$(^3P)3p\ ^4D^\circ_{3/2}$	$(^3P)3d\ ^2D_{3/2}$	3248.1314
30816.35426	0.12	0.058	0.088	0.14	14	2.5	< 71	$(^3P)3p\ ^4D^\circ_{5/2}$	$(^3P)3d\ ^2F_{7/2}$	3244.0941
30822.98282	0.16	0.45	0.49	−0.15	14	1.7	< 166	$(^3P)3p\ ^4D^\circ_{5/2}$	$(^3P)3d\ ^2D_{5/2}$	3243.3965
30928.09321	0.11	0.036	0.053	0.002	10	2.8	158	$(^1D)3s\ ^2D_{3/2}$	$(^1D)3p\ ^2D^\circ_{3/2}$	3232.3733
30928.89075[g]	0.26	3.2	3.2	6.0	4	0.9		$(^3P)3p\ ^4D^\circ_{1/2}$	$(^3P)3d\ ^4P_{1/2}$	3232.2899
30931.45428	0.13	0.12	0.12	−0.19	18	2.1	158	$(^1D)3s\ ^2D_{5/2}$	$(^1D)3p\ ^2D^\circ_{3/2}$	3232.0220
30946.78549	0.13	0.14	0.16	−0.09	19	2.1	158	$(^1D)3s\ ^2D_{3/2}$	$(^1D)3p\ ^2D^\circ_{5/2}$	3230.4208
30950.14656	0.10	0.025	0.035	0.012	9	3.0	158	$(^1D)3s\ ^2D_{5/2}$	$(^1D)3p\ ^2D^\circ_{5/2}$	3230.0700
30954.92344	0.12	0.034	0.038		12	2.7	< 71	$(^1D)3p\ ^2F^\circ_{7/2}$	$(^1D)3d\ ^2G_{9/2}$	3229.5715
30956.03345	0.21	1.0	1.6	−3.3	12	1.3		$(^1D)3p\ ^2F^\circ_{7/2}$	$(^1D)3d\ ^2G_{7/2}$	3229.4557
31000.55782	0.13	0.039	0.049	−0.009	15	2.7	< 76	$(^1D)3p\ ^2F^\circ_{5/2}$	$(^1D)3d\ ^2G_{7/2}$	3224.8172
31064.37486	0.13	0.039	0.046		12	2.7	< 60	$(^3P)3p\ ^4D^\circ_{7/2}$	$(^3P)3d\ ^4F_{9/2}$	3218.1921
31073.00361[g]	0.25	4.6	4.6	−11	4	0.6		$(^3P)3p\ ^4D^\circ_{3/2}$	$(^3P)3d\ ^4P_{1/2}$	3217.2984
31095.93236	0.15	1.6	1.6	1.1	11	1.0		$(^3P)3p\ ^2S^\circ_{1/2}$	$(^3P)4s\ ^2P_{1/2}$	3214.9260
31097.5743	4.3	2.4	2.8		9	0.8		$(^1S)3s\ ^2S_{1/2}$	$(^3P)5p\ ^4D^\circ_{3/2}$	3214.7563
31101.73516	0.11	0.045	0.045	−0.075	13	2.7	< 71	$(^3P)3p\ ^4D^\circ_{3/2}$	$(^3P)3d\ ^4F_{5/2}$	3214.3262
31107.45968	0.14	0.091	0.091	−0.15	17	2.4	< 66	$(^3P)3p\ ^4D^\circ_{1/2}$	$(^3P)3d\ ^4F_{3/2}$	3213.7346
31149.90549	0.18	0.14	0.17	−0.17	19	2.1	< 76	$(^3P)3p\ ^4D^\circ_{1/2}$	$(^3P)3d\ ^4P_{3/2}$	3209.3554
31153.70306	0.17	0.40	0.57	0.07	18	1.7	< 135	$(^3P)3p\ ^4D^\circ_{7/2}$	$(^3P)3d\ ^2F_{7/2}$	3208.9641
31251.57254	0.17	2.4	3.2	−0.26	12	0.9		$(^3P)3p\ ^4D^\circ_{3/2}$	$(^3P)3d\ ^4F_{3/2}$	3198.9144
31254.78308	0.11	0.049	0.062	0.19	18	2.7	< 67	$(^3P)3p\ ^4D^\circ_{5/2}$	$(^3P)3d\ ^4F_{7/2}$	3198.5858
31294.01835	0.18	0.16	0.19	−0.04	14	2.0	< 71	$(^3P)3p\ ^4D^\circ_{3/2}$	$(^3P)3d\ ^4P_{3/2}$	3194.5753
31329.750	10	5.7	6.6		5	0.5		$(^1S)3s\ ^2S_{1/2}$	$(^3P)5p\ ^2S^\circ_{1/2}$	3190.9318
31330.42968	0.16	0.56	0.56	1.2	13	1.6	< 142	$(^3P)3p\ ^4D^\circ_{3/2}$	$(^3P)3d\ ^2F_{5/2}$	3190.8626
31351.27725	0.14	0.25	0.26	−0.29	17	1.8	< 84	$(^3P)3p\ ^4D^\circ_{5/2}$	$(^3P)3d\ ^4F_{5/2}$	3188.7407
31362.72428	0.12	0.73	0.73	1.8	10	1.3	127	$(^3P)3s\ ^4P_{3/2}$	$(^3P)3p\ ^2D^\circ_{5/2}$	3187.5768
31459.7532	9.2	6.0	6.0		4	0.5		$(^1S)3s\ ^2S_{1/2}$	$(^3P)5p\ ^4S^\circ_{3/2}$	3177.7452
31475.85249	0.14	0.70	0.70	−0.15	18	1.4		$(^3P)3p\ ^4D^\circ_{3/2}$	$(^3P)3d\ ^4P_{5/2}$	3176.1198
31500.0662	5.0	3.1	3.3		8	0.8		$(^1S)3s\ ^2S_{1/2}$	$(^3P)5p\ ^2D^\circ_{3/2}$	3173.6783
31501.11464	0.17	0.81	0.90	1.5	12	1.4		$(^3P)3p\ ^4D^\circ_{5/2}$	$(^3P)3d\ ^4F_{3/2}$	3173.5726
31574.65137	0.14	3.3	3.3	−4.0	5	0.7		$(^3P)3s\ ^4P_{1/2}$	$(^3P)3p\ ^2D^\circ_{3/2}$	3166.1812
31579.97178	0.16	0.38	0.38	0.43	16	1.7	< 100	$(^3P)3p\ ^4D^\circ_{5/2}$	$(^3P)3d\ ^2F_{5/2}$	3165.6477

Table 3. *Continued.*

σ^a_{Ritz} (cm^{-1})	$u^{a,b}_{Ritz}$	u^b_{wm} (10^{-3} cm^{-1})	u^b_ϵ	$\sigma_{Ritz}-\sigma_\epsilon$	spec^c	S/N^d (log)	IS^e (10^{-3})	Transition Lower	Upper	λ^f (Å)
31589.80946	0.15	0.12	0.12	−0.17	15	2.1	< 86	$(^1D)3p\ ^2P^\circ_{1/2}$	$(^1D)4s\ ^2D_{3/2}$	3164.6618
31592.13189	0.16	0.60	0.67	−0.17	14	1.5	< 181	$(^3P)3p\ ^4D^\circ_{7/2}$	$(^3P)3d\ ^4F_{7/2}$	3164.4292
31688.62606	0.17	3.5	5.0	3.0	6	0.7		$(^3P)3p\ ^4D^\circ_{7/2}$	$(^3P)3d\ ^4F_{5/2}$	3154.7929
31725.39458	0.14	0.80	1.2	2.8	11	1.3		$(^3P)3p\ ^4D^\circ_{5/2}$	$(^3P)3d\ ^4P_{5/2}$	3151.1365
31800.23440	0.13	0.31	0.34	0.49	16	1.7	< 110	$(^3P)3p\ ^2D^\circ_{3/2}$	$(^3P)4s\ ^2P_{3/2}$	3143.7202
31824.41364	0.13	0.075	0.10	−0.23	15	2.3	< 75	$(^1D)3p\ ^2P^\circ_{3/2}$	$(^1D)4s\ ^2D_{5/2}$	3141.3316
31824.77281[g]	0.16	0.61	0.61	1.0	9	1.4	< 165	$(^1D)3p\ ^2P^\circ_{3/2}$	$(^1D)4s\ ^2D_{3/2}$	3141.2962
31834.32402	0.18	3.8	5.4	−4.4	8	0.5		$(^1D)3p\ ^2F^\circ_{7/2}$	$(^1D)3d\ ^2D_{5/2}$	3140.3537
31873.67021	0.13	3.7	3.7	−6.2	5	0.6		$(^3P)3s\ ^4P_{3/2}$	$(^3P)3p\ ^2D^\circ_{3/2}$	3136.4769
31880.38866	0.13	2.3	2.3	−4.5	7	0.9		$(^3P)3s\ ^4P_{5/2}$	$(^3P)3p\ ^2D^\circ_{5/2}$	3135.8159
31898.19453	0.21	5.8	5.9	9.0	4	0.5		$(^1D)3p\ ^2F^\circ_{5/2}$	$(^1D)3d\ ^2D_{3/2}$	3134.0654
31917.32058	0.18	1.0	1.1	1.0	13	1.2		$(^3P)3p\ ^4D^\circ_{7/2}$	$(^3P)3d\ ^2F_{5/2}$	3132.1873
32060.89416	0.14	0.094	0.094		21	2.3		$(^1S)3s\ ^2S_{1/2}$	$(^3P)5p\ ^2P^\circ_{3/2}$	3118.1603
32062.74339	0.16	0.20	0.51	1.0	18	1.9	< 78	$(^3P)3p\ ^4D^\circ_{7/2}$	$(^3P)3d\ ^4P_{5/2}$	3117.9805
32274.31216	0.17	8.2	13	2.5	3	0.4		$(^3P)3p\ ^4D^\circ_{5/2}$	$(^3P)3d\ ^2P_{3/2}$	3097.5403
32278.57463	0.17	0.19	0.24	0.11	18	1.9	< 84	$(^1D)3p\ ^2F^\circ_{7/2}$	$(^1D)3d\ ^2F_{7/2}$	3097.1313
32299.71839	0.16	0.16	0.16		17	2.0		$(^1S)3s\ ^2S_{1/2}$	$(^3P)5p\ ^2P^\circ_{1/2}$	3095.1038
32311.18033	0.11	0.075	0.075	−0.18	11	2.4	< 75	$(^3P)3p\ ^2D^\circ_{5/2}$	$(^3P)4s\ ^2P_{3/2}$	3094.0058
32322.71357	0.23	0.55	0.55	−0.30	2	1.7	< 109	$(^1D)3p\ ^2F^\circ_{5/2}$	$(^1D)3d\ ^2F_{5/2}$	3092.9017
32372.29933	0.13	0.10	0.10	0.16	16	2.2	< 84	$(^3P)3p\ ^2D^\circ_{3/2}$	$(^3P)4s\ ^2P_{1/2}$	3088.1641
32552.30336	0.19	1.6	1.7	−0.64	12	1.1		$(^3P)3p\ ^4D^\circ_{5/2}$	$(^3P)4s\ ^4P_{5/2}$	3071.0868
32679.80202	0.18	0.42	0.51	−0.82	16	1.6	< 81	$(^3P)3p\ ^4D^\circ_{3/2}$	$(^3P)4s\ ^4P_{3/2}$	3059.1046
32727.19410	0.20	0.24	0.28	$< 10^{-3}$	24	1.9	< 84	$(^3P)3p\ ^4P^\circ_{1/2}$	$(^3P)3d\ ^4D_{3/2}$	3054.6746
32803.62964	0.15	0.093	0.12	0.27	19	2.3	< 86	$(^3P)3p\ ^4P^\circ_{3/2}$	$(^3P)3d\ ^4D_{5/2}$	3047.5566
32825.18953	0.29	0.20	0.20	−0.10	25	1.9	< 94	$(^3P)3p\ ^4P^\circ_{1/2}$	$(^3P)3d\ ^4D_{1/2}$	3045.5549
32841.01273	0.27	0.44	0.44	−0.67	15	1.7	< 154	$(^3P)3p\ ^4D^\circ_{1/2}$	$(^3P)4s\ ^4P_{1/2}$	3044.0874
32889.65217	0.18	0.18	0.18	−0.28	19	2.1	< 65	$(^3P)3p\ ^4D^\circ_{7/2}$	$(^3P)4s\ ^4P_{5/2}$	3039.5854
32909.86126	0.18	0.12	0.12	−0.02	25	2.2	< 55	$(^3P)3p\ ^4P^\circ_{3/2}$	$(^3P)3d\ ^4D_{3/2}$	3037.7188
32929.34411	0.17	0.15	0.15	−0.36	18	2.0	< 74	$(^3P)3p\ ^4D^\circ_{5/2}$	$(^3P)4s\ ^4P_{3/2}$	3035.9215
32945.19366	0.11	0.051	0.051	0.050	24	2.6	< 60	$(^3P)3p\ ^4P^\circ_{5/2}$	$(^3P)3d\ ^4D_{7/2}$	3034.4609
32985.12559	0.26	0.35	0.35	0.14	19	1.7	< 134	$(^3P)3p\ ^4D^\circ_{3/2}$	$(^3P)4s\ ^4P_{1/2}$	3030.7872
33006.07278	0.11	0.14	0.20	−0.19	27	2.1	118	$(^3P)3s\ ^4P_{1/2}$	$(^3P)3p\ ^4S^\circ_{3/2}$	3028.8636
33007.85668	0.31	0.70	0.70	1.3	15	1.4		$(^3P)3p\ ^4P^\circ_{3/2}$	$(^3P)3d\ ^4D_{1/2}$	3028.6999
33026.23067	0.16	0.13	0.17	0.04	22	2.1	< 90	$(^3P)3p\ ^4P^\circ_{5/2}$	$(^3P)3d\ ^4D_{5/2}$	3027.0148
33132.46229	0.20	0.77	0.77	0.51	21	1.3		$(^3P)3p\ ^4P^\circ_{5/2}$	$(^3P)3d\ ^4D_{3/2}$	3017.3090
33305.09163	0.10	0.097	0.11	−0.36	25	2.2	120	$(^3P)3s\ ^4P_{3/2}$	$(^3P)3p\ ^4S^\circ_{3/2}$	3001.6688
33380.2581	4.5	4.8	5.5	12	3	0.6		$(^1S)3p\ ^2P^\circ_{1/2}$	$(^1S)4s\ ^2S_{1/2}$	2994.9093
33390.1502	4.5	3.5	3.5	−4.8	7	0.7		$(^1S)3p\ ^2P^\circ_{3/2}$	$(^1S)4s\ ^2S_{1/2}$	2994.0220
33692.16288	0.12	0.078	0.079	−0.19	21	2.3	< 78	$(^1D)3p\ ^2F^\circ_{7/2}$	$(^1D)4s\ ^2D_{5/2}$	2967.1828
33736.68724[g]	0.16	2.0	2.3	3.1	6	1.0		$(^1D)3p\ ^2F^\circ_{5/2}$	$(^1D)4s\ ^2D_{5/2}$	2963.2666
33737.04642	0.14	0.099	0.099	0.20	17	2.2	< 87	$(^1D)3p\ ^2F^\circ_{5/2}$	$(^1D)4s\ ^2D_{3/2}$	2963.2351
33822.75601	0.11	0.096	0.096	−0.026	17	2.3	121	$(^3P)3s\ ^4P_{5/2}$	$(^3P)3p\ ^4S^\circ_{3/2}$	2955.7257
34058.54360	0.20	12	12	23	2	0.5		$(^3P)3p\ ^4P^\circ_{3/2}$	$(^3P)3d\ ^2D_{3/2}$	2935.2623
34076.53304	0.17	6.2	6.2	−1.0	5	0.8		$(^3P)3p\ ^4P^\circ_{5/2}$	$(^3P)3d\ ^2D_{5/2}$	2933.7126
34170.82774	0.25	1.6	1.6	−1.4	20	1.3		$(^3P)3p\ ^4P^\circ_{1/2}$	$(^3P)3d\ ^4P_{1/2}$	2925.6167
34217.54310	0.14	11	11	−29	3	0.7		$(^3P)3s\ ^4P_{1/2}$	$(^3P)3p\ ^2P^\circ_{3/2}$	2921.6223
34281.14463	0.21	5.4	6.0	−9.2	7	0.6		$(^3P)3p\ ^4P^\circ_{5/2}$	$(^3P)3d\ ^2D_{3/2}$	2916.2016
34349.39667	0.17	0.65	0.69	−0.07	22	1.8	< 298	$(^3P)3p\ ^4P^\circ_{1/2}$	$(^3P)3d\ ^4F_{3/2}$	2910.4068
34353.49489	0.24	0.60	0.60	1.3	23	1.8	< 310	$(^3P)3p\ ^4P^\circ_{3/2}$	$(^3P)3d\ ^4P_{1/2}$	2910.0596
34382.22644[g]	0.14	10	11	5.9	3	0.3		$(^3P)3p\ ^4P^\circ_{3/2}$	$(^3P)3d\ ^4F_{5/2}$	2907.6277
34391.84248	0.19	1.2	1.4	1.2	21	1.3		$(^3P)3p\ ^4P^\circ_{1/2}$	$(^3P)3d\ ^4P_{3/2}$	2906.8147
34508.33330	0.15	3.1	3.1	−6.4	14	1.1		$(^3P)3p\ ^4P^\circ_{5/2}$	$(^3P)3d\ ^4F_{7/2}$	2897.0016
34574.50963	0.19	36	36	−11	1	0.5		$(^3P)3p\ ^4P^\circ_{3/2}$	$(^3P)3d\ ^4P_{3/2}$	2891.4565
34610.92096	0.16	4.8	4.8	−1.0	7	0.9		$(^3P)3p\ ^4P^\circ_{3/2}$	$(^3P)3d\ ^2F_{5/2}$	2888.4144

Table 3. *Continued.*

σ^a_{Ritz} (cm^{-1})	$u^{a,b}_{Ritz}$	u^b_{wm} (10^{-3} cm^{-1})	u^b_ϵ	$\sigma_{Ritz}-\sigma_\epsilon$	spec^c	S/N^d (log)	IS^e (10^{-3})	Transition Lower	Upper	λ^f (Å)
34734.84101	0.33	13	26	11	3	0.6		$(^3P)3p\ ^4P^\circ_{1/2}$	$(^3P)3d\ ^2P_{1/2}$	2878.1093
34754.66486	0.17	1.0	1.2	0.2	19	1.6	< 379	$(^3P)3p\ ^4P^\circ_{5/2}$	$(^3P)3d\ ^4F_{3/2}$	2876.4675
34756.34377	0.14	0.81	0.81	−0.31	21	1.6	< 320	$(^3P)3p\ ^4P^\circ_{3/2}$	$(^3P)3d\ ^4P_{5/2}$	2876.3286
34797.11066	0.19	1.6	1.8	−2.6	17	1.3		$(^3P)3p\ ^4P^\circ_{5/2}$	$(^3P)3d\ ^4P_{3/2}$	2872.9586
34833.52200	0.17	2.1	2.3	−3.2	13	1.3		$(^3P)3p\ ^4P^\circ_{5/2}$	$(^3P)3d\ ^2F_{5/2}$	2869.9554
34978.94480	0.15	1.8	1.8	1.4	16	1.3		$(^3P)3p\ ^4P^\circ_{5/2}$	$(^3P)3d\ ^4P_{5/2}$	2858.0231
35034.22633	0.13	6.7	7.2	−12	6	0.7		$(^3P)3s\ ^4P_{5/2}$	$(^3P)3p\ ^2P^\circ_{3/2}$	2853.5132
35583.25255	0.19	0.17	0.26	−0.08	21	2.7	< 101	$(^3P)3p\ ^4P^\circ_{3/2}$	$(^3P)4s\ ^4P_{5/2}$	2809.4832
35777.62614	0.17	0.18	0.18	0.59	26	2.6	< 178	$(^3P)3p\ ^4P^\circ_{1/2}$	$(^3P)4s\ ^4P_{3/2}$	2794.2190
35805.85358	0.17	0.13	0.14	0.16	22	3.0	< 101	$(^3P)3p\ ^4P^\circ_{5/2}$	$(^3P)4s\ ^4P_{5/2}$	2792.0161
35960.29330	0.17	0.70	0.73	−0.44	13	1.9	< 296	$(^3P)3p\ ^4P^\circ_{3/2}$	$(^3P)4s\ ^4P_{3/2}$	2780.0245
36082.94971	0.26	0.66	0.66	−0.02	18	1.9	< 276	$(^3P)3p\ ^4P^\circ_{1/2}$	$(^3P)4s\ ^4P_{1/2}$	2770.5739
36182.89433	0.17	0.18	0.18	0.23	27	2.6	< 102	$(^3P)3p\ ^4P^\circ_{5/2}$	$(^3P)4s\ ^4P_{3/2}$	2762.9206
36265.61687	0.25	0.19	0.19	−0.01	23	2.6	< 111	$(^3P)3p\ ^4P^\circ_{3/2}$	$(^3P)4s\ ^4P_{1/2}$	2756.6180
36724.65050	0.17	1.4	1.4	−0.8	13	1.5	< 380	$(^3P)3p\ ^4P^\circ_{1/2}$	$(^3P)4s\ ^2P_{3/2}$	2722.1603
37117.3992	2.0	1.2	1.3	−0.5	9	1.4		$2s2p^6\ ^2S_{1/2}$	$(^3P)3p\ ^2P^\circ_{3/2}$	2693.3548
37129.91869	0.16	1.5	1.6	4.2	9	1.4	< 366	$(^3P)3p\ ^4P^\circ_{5/2}$	$(^3P)4s\ ^2P_{3/2}$	2692.4466
37244.5795	2.0	8.4	8.6	10	6	0.7		$2s2p^6\ ^2S_{1/2}$	$(^3P)3p\ ^2P^\circ_{1/2}$	2684.1572
40985.9909	5.1	2.5	3.3		11	1.1		$(^1S)3s\ ^2S_{1/2}$	$(^1D)4p\ ^2P^\circ_{3/2}$	2439.1185
41151.195	14	9.4	9.4		2	0.6		$(^1S)3s\ ^2S_{1/2}$	$(^1D)4p\ ^2P^\circ_{1/2}$	2429.3257
45639.010	12	7.7	7.9		6	0.7		$(^1D)3s\ ^2D_{5/2}$	$(^3P)4p\ ^2D^\circ_{5/2}$	2190.4231
46054.2787	5.8	4.1	4.1	−1.0	9	1.0		$(^1D)3s\ ^2D_{3/2}$	$(^3P)4p\ ^2D^\circ_{3/2}$	2170.6701
46057.6397	5.8	9.8	9.8	4.8	5	0.7		$(^1D)3s\ ^2D_{5/2}$	$(^3P)4p\ ^2D^\circ_{3/2}$	2170.5117
46149.2135	8.9	5.8	5.8		9	0.9		$(^1D)3s\ ^2D_{3/2}$	$(^3P)4p\ ^2S^\circ_{1/2}$	2166.2043
47688.98016	0.78	0.54	0.78	0.16	5	1.9	194	$(^1D)3s\ ^2D_{3/2}$	$(^3P)4p\ ^2P^\circ_{3/2}$	2096.2546
47692.34123	0.78	0.29	0.66	−0.09	4	2.9	194	$(^1D)3s\ ^2D_{5/2}$	$(^3P)4p\ ^2P^\circ_{3/2}$	2096.1068
47935.70871	0.85	0.29	0.55		5	2.6	195	$(^1D)3s\ ^2D_{3/2}$	$(^3P)4p\ ^2P^\circ_{1/2}$	2085.4637
51290.07993	0.70	14	30	$< 10^{-2}$	2	0.5		$(^3P)3p\ ^2P^\circ_{1/2}$	$(^1D)3d\ ^2P_{1/2}$	1949.6948
51401.93314	0.64	13	13	8	4	0.6		$(^3P)3p\ ^2P^\circ_{3/2}$	$(^1D)3d\ ^2P_{3/2}$	1945.4521
51577.56111	0.58	0.83	1.1	0.4	5	1.7	231	$(^3P)3s\ ^2P_{1/2}$	$(^1D)3p\ ^2P^\circ_{3/2}$	1938.8276
51718.88644	0.60	9.7	26	45	4	0.6		$(^3P)3p\ ^2P^\circ_{1/2}$	$(^1D)3d\ ^2S_{1/2}$	1933.5296
51812.52446	0.58	0.52	0.55	−0.42	5	2.0	231	$(^3P)3s\ ^2P_{1/2}$	$(^1D)3p\ ^2P^\circ_{1/2}$	1930.0353
51846.06674	0.60	10	10	14	4	0.8		$(^3P)3p\ ^2P^\circ_{3/2}$	$(^1D)3d\ ^2S_{1/2}$	1928.7866
51970.58517	0.61	72	72	15	1	0.1		$(^3P)3p\ ^2P^\circ_{1/2}$	$(^1D)3d\ ^2D_{3/2}$	1924.1654
52078.41933	0.60	43	43	−45	1	0.4		$(^3P)3p\ ^2P^\circ_{3/2}$	$(^1D)3d\ ^2D_{5/2}$	1920.1812
52189.82482	0.58	0.38	0.62	0.49	5	2.2	233	$(^3P)3s\ ^2P_{3/2}$	$(^1D)3p\ ^2P^\circ_{3/2}$	1916.0823
52424.78817	0.58	1.3	1.3	−0.2	5	1.5	233	$(^3P)3s\ ^2P_{3/2}$	$(^1D)3p\ ^2P^\circ_{1/2}$	1907.4946

[a]Ritz wavenumbers and uncertainties for ^{20}Ne derived with error corrections of $k_1 = 1.53$ and $k_2 = 7.5 \times 10^{-5}$ cm^{-1}. [b]One standard deviation uncertainties, given with two significant digits to make the steps in the analysis possible to follow. [c]Number of lines used to calculate σ_ϵ. [d]Lowest intensity of the lines used to calculate σ_ϵ. [e]In units of cm^{-1}. Also includes estimated conservative upper limits to transitions without visible IS. [f]Air wavelengths above 2000 Å, calculated with refractive index of air from [23], vacuum wavelengths below 2000 Å. [g]Transition not found in prior works.

an unidentified blend was suspected, it was removed from the mean. In spite of this, an ϵ of about the same size as the uncertainty of the weighted mean had to be employed for many lines, especially those with high S/N, resulting in $u_\epsilon > u_{wm}$ in Tables 3 and 4. For transitions with 3s lower levels, the non-zero ϵ can to some degree also be explained by the two effects discussed above. Great care was taken when correcting the phase of the interferograms. However, small errors are introduced in the approximations used, which will result in asymmetric line profiles. This in turn contributes to an error in the line center positions, since the fitting routines are based on symmetric functions.

Shift in wavenumber due to the illumination of the FTS aperture has been investigated in [11]. They occur if the cylindrical plasma of a HC source is imaged onto the aperture and the intensity of the calibration lines have a radial distribution that differs from that of the investigated lines. The effect has been minimized by the optics used in the experimental setup, see Section 2, and should be further reduced by the fact that both the calibration

Table 4. Finding list for observed Ne III 3s–3p and 3p–3d transitions.

σ^a_{Ritz} (cm^{-1})	$u^{a,b}_{Ritz}$	u^b_{wm} (10^{-3} cm^{-1})	u^b_ϵ (10^{-3} cm^{-1})	$\sigma_{Ritz}-\sigma_\epsilon$	spec^c	S/N^d (log)	IS^e (10^{-3})	Transition Lower	Transition Upper	λ^f (Å)
24579.2241	5.0	3.1	3.2	$< 10^{-3}$	1	0.9		$(^2P^\circ)3s\ ^3P^\circ_1$	$(^2D^\circ)3p\ ^3P_1$	4067.3281
26506.0515	2.6	1.7	1.7	$< 10^{-3}$	4	1.2	261	$(^2P^\circ)3s\ ^1P^\circ_1$	$(^2D^\circ)3p\ ^1D_2$	3771.6518
30033.15698	0.30	0.19	0.19	$< 10^{-3}$	5	2.2	374	$(^2D^\circ)3s\ ^1D^\circ_2$	$(^2D^\circ)3p\ ^1P_1$	3328.6957
34402.7727	2.5	1.5	1.6	$< 10^{-3}$	12	1.3	318	$(^2P^\circ)3s\ ^1P^\circ_1$	$(^2P^\circ)3p\ ^1P_1$	2905.8911
34779.004	16	6.3	12	3	4	0.6		$(^2D^\circ)3s\ ^3D^\circ_1$	$(^2D^\circ)3p\ ^1P_1$	2874.4544
34872.83965	0.42	0.27	0.27	$< 10^{-2}$	16	2.1	367	$(^2D^\circ)3s\ ^1D^\circ_2$	$(^2D^\circ)3p\ ^1F_3$	2866.7195
35377.2556	2.5	1.8	1.8	−1.0	13	1.3	249	$(^2P^\circ)3s\ ^3P^\circ_2$	$(^2P^\circ)3p\ ^3S_1$	2825.8432
35383.1642	4.4	8.1	8.1	−6.9	4	0.7		$(^2P^\circ)3s\ ^3P^\circ_0$	$(^2P^\circ)3p\ ^3S_1$	2825.3713
35383.8177	2.6	3.2	3.4	5.0	9	1.1		$(^2P^\circ)3s\ ^3P^\circ_1$	$(^2P^\circ)3p\ ^3S_1$	2825.3192
35861.39673	0.74	0.47	0.52	0.31	15	1.9	289	$(^2D^\circ)3s\ ^3D^\circ_1$	$(^2D^\circ)3p\ ^3D_1$	2787.6915
35872.3852	1.0	1.8	1.8	2.1	11	1.4	292	$(^2D^\circ)3s\ ^3D^\circ_1$	$(^2D^\circ)3p\ ^3D_2$	2786.8375
35881.5298	1.1	1.3	1.3	1.6	12	1.5	272	$(^2D^\circ)3s\ ^3D^\circ_2$	$(^2D^\circ)3p\ ^3D_1$	2786.1272
35892.51832	0.56	0.33	0.38	−0.02	13	2.1	275	$(^2D^\circ)3s\ ^3D^\circ_2$	$(^2D^\circ)3p\ ^3D_2$	2785.2742
35921.9448	1.0	1.5	2.2	−1.0	11	1.4	273	$(^2D^\circ)3s\ ^3D^\circ_3$	$(^2D^\circ)3p\ ^3D_2$	2782.9925
35961.8760	1.0	1.8	2.3	3.3	11	1.3	283	$(^2D^\circ)3s\ ^3D^\circ_2$	$(^2D^\circ)3p\ ^3D_3$	2779.9021
35991.30256	0.30	0.20	0.20	−0.04	16	2.4	281	$(^2D^\circ)3s\ ^3D^\circ_3$	$(^2D^\circ)3p\ ^3D_3$	2777.6292
37320.57314	0.32	0.16	0.21	$< 10^{-2}$	14	2.8	394	$(^4S^\circ)3s\ ^3S^\circ_1$	$(^4S^\circ)3p\ ^3P_1$	2678.6913
37330.6047	2.6	1.7	1.7	−0.1	3	2.3	388	$(^4S^\circ)3s\ ^3S^\circ_1$	$(^4S^\circ)3p\ ^3P_0$	2677.9715
37331.53263	0.69	0.45	0.45	$< 10^{-2}$	4	3.0	394	$(^4S^\circ)3s\ ^3S^\circ_1$	$(^4S^\circ)3p\ ^3P_2$	2677.9049
37851.97342	0.42	0.24	0.27	0.01	10	2.4	273	$(^2P^\circ)3s\ ^3P^\circ_2$	$(^2P^\circ)3p\ ^3D_3$	2641.0833
37859.442	14	8.2	13	5	4	0.7		$(^2D^\circ)3p\ ^3P_2$	$(^2D^\circ)3d\ ^3D^\circ_3$	2640.5622
37879.4357	1.4	1.1	1.1	−0.3	12	1.6	253	$(^2P^\circ)3s\ ^3P^\circ_2$	$(^2P^\circ)3p\ ^3D_2$	2639.1684
37885.9979	1.6	1.8	1.8	0.2	3	1.7	254	$(^2P^\circ)3s\ ^3P^\circ_1$	$(^2P^\circ)3p\ ^3D_2$	2638.7112
37886.3556	6.3	5.3	5.4	10	1	1.6	279	$(^2P^\circ)3s\ ^3P^\circ_0$	$(^2P^\circ)3p\ ^3D_1$	2638.6863
37887.0091	6.4	2.5	5.9	−12	3	1.3	284	$(^2P^\circ)3s\ ^3P^\circ_1$	$(^2P^\circ)3p\ ^3D_1$	2638.6408
38217.07897	0.56	0.22	0.38	−0.27	12	2.4	276	$(^2D^\circ)3s\ ^3D^\circ_1$	$(^2D^\circ)3p\ ^3F_2$	2615.8503
38237.2121	1.0	1.1	1.1	0.2	12	1.6	259	$(^2D^\circ)3s\ ^3D^\circ_2$	$(^2D^\circ)3p\ ^3F_2$	2614.4728
38252.66750	0.44	0.18	0.29	$< 10^{-2}$	12	2.6	275	$(^2D^\circ)3s\ ^3D^\circ_2$	$(^2D^\circ)3p\ ^3F_3$	2613.4164
38282.0939	1.0	1.3	1.5	−0.7	9	1.5	273	$(^2D^\circ)3s\ ^3D^\circ_3$	$(^2D^\circ)3p\ ^3F_3$	2611.4075
38302.64790	0.35	0.17	0.23	$< 10^{-2}$	11	2.7	272	$(^2D^\circ)3s\ ^3D^\circ_3$	$(^2D^\circ)3p\ ^3F_4$	2610.0060
38514.47493	0.56	0.26	0.36	−0.03	12	2.4	230	$(^4S^\circ)3s\ ^5S^\circ_2$	$(^4S^\circ)3p\ ^5P_1$	2595.6503
38545.57965	0.54	0.20	0.35	0.04	11	2.6	233	$(^4S^\circ)3s\ ^5S^\circ_2$	$(^4S^\circ)3p\ ^5P_2$	2593.5556
38598.52935	0.45	0.18	0.30	−0.01	11	2.7	232	$(^4S^\circ)3s\ ^5S^\circ_2$	$(^4S^\circ)3p\ ^5P_3$	2589.9975
39638.820	16	18	75	−40	2	0.4		$(^2D^\circ)3s\ ^3D^\circ_2$	$(^2D^\circ)3p\ ^1F_3$	2522.0206
39875.4301	7.8	3.6	5.1		6	1.1		$(^2P^\circ)3p\ ^1D_2$	$(^2P^\circ)3d\ ^1F^\circ_3$	2507.0546
40418.18248	0.47	0.15	0.30	$< 10^{-3}$	11	3.2	311	$(^2P^\circ)3s\ ^1P^\circ_1$	$(^2P^\circ)3p\ ^1D_2$	2473.3865
40600.342	11	7.3	7.3		6	0.8		$(^2D^\circ)3p\ ^3P_2$	$(^2D^\circ)3d\ ^3P^\circ_2$	2462.2885
40626.076	38	33	33	38	1	0.4		$(^2D^\circ)3p\ ^3P_1$	$(^2D^\circ)3d\ ^3P^\circ_1$	2460.7286
40679.050	16	11	11		2	0.5		$(^2D^\circ)3p\ ^3P_1$	$(^2D^\circ)3d\ ^3P^\circ_0$	2457.5240
40722.091	38	18	37	−47	2	0.6		$(^2D^\circ)3p\ ^3P_2$	$(^2D^\circ)3d\ ^3P^\circ_1$	2454.9263
40982.9260	3.0	1.9	1.9		5	1.3		$(^2D^\circ)3p\ ^3P_1$	$(^2D^\circ)3d\ ^3S^\circ_1$	2439.3009
41416.216	12	7.9	10	−6	5	0.9		$(^4S^\circ)3p\ ^3P_0$	$(^4S^\circ)3d\ ^3D^\circ_1$	2413.7794
41420.0018	4.1	8.2	8.2	1.1	6	0.8		$(^4S^\circ)3p\ ^3P_2$	$(^4S^\circ)3d\ ^3D^\circ_2$	2413.5587
41426.248	12	7.4	12	8	4	0.9		$(^4S^\circ)3p\ ^3P_1$	$(^4S^\circ)3d\ ^3D^\circ_1$	2413.1948
41430.9612	4.0	2.7	2.7	−0.1	10	1.2		$(^4S^\circ)3p\ ^3P_1$	$(^4S^\circ)3d\ ^3D^\circ_2$	2412.9203
41432.7214	3.0	1.5	2.0		11	1.5	< 465	$(^4S^\circ)3p\ ^3P_2$	$(^4S^\circ)3d\ ^3D^\circ_3$	2412.8177
41533.282	12	8.3	8.4		1	0.8		$(^2P^\circ)3p\ ^3P_1$	$(^2P^\circ)3d\ ^3P^\circ_0$	2406.9753
41537.333	39	25	25		1	0.4		$(^2P^\circ)3p\ ^3P_2$	$(^2P^\circ)3d\ ^3P^\circ_1$	2406.7406
41644.376	10	7.1	7.1	−7.1	5	0.7		$(^2P^\circ)3p\ ^3P_2$	$(^2P^\circ)3d\ ^3P^\circ_2$	2400.5538
41689.394	10	15	24	8	3	0.5		$(^2P^\circ)3p\ ^3P_1$	$(^2P^\circ)3d\ ^3P^\circ_2$	2397.9614
42233.9346	4.1	1.5	2.6	$< 10^{-3}$	3	1.5	275	$(^2P^\circ)3s\ ^3P^\circ_1$	$(^2P^\circ)3p\ ^3P_0$	2367.0410
42256.98738	0.86	0.29	0.58	0.19	12	2.3	260	$(^2P^\circ)3s\ ^3P^\circ_2$	$(^2P^\circ)3p\ ^3P_1$	2365.7496
42262.8960	3.7	2.6	2.6	−1.7	2	2.2	256	$(^2P^\circ)3s\ ^3P^\circ_0$	$(^2P^\circ)3p\ ^3P_1$	2365.4188
42263.5495	1.3	2.8	2.9	−2.4	2	2.1	261	$(^2P^\circ)3s\ ^3P^\circ_1$	$(^2P^\circ)3p\ ^3P_1$	2365.3822
42302.00512	0.53	0.18	0.35	−0.03	12	2.7	262	$(^2P^\circ)3s\ ^3P^\circ_2$	$(^2P^\circ)3p\ ^3P_2$	2363.2317

Table 4. *Continued.*

σ^a_{Ritz} (cm^{-1})	$u^{a,b}_{Ritz}$	u^b_{wm} (10^{-3} cm^{-1})	u^b_ϵ	$\sigma_{Ritz}-\sigma_\epsilon$	spec[c]	S/N^d (log)	IS^e (10^{-3})	Transition Lower	Upper	λ^f (Å)
42308.56728	0.92	0.31	0.65	0.06	12	2.2	263	$(^2P^\circ)3s\ ^3P^\circ_1$	$(^2P^\circ)3p\ ^3P_2$	2362.8652
43328.765	12	19	19	10	3	0.5		$(^2P^\circ)3p\ ^3P_2$	$(^2P^\circ)3d\ ^3D^\circ_2$	2307.2256
43340.7421	8.7	3.8	5.7		7	1.0		$(^2P^\circ)3p\ ^3P_2$	$(^2P^\circ)3d\ ^3D^\circ_3$	2306.5880
43373.783	12	7.0	8.8	−2.1	5	0.8		$(^2P^\circ)3p\ ^3P_1$	$(^2P^\circ)3d\ ^3D^\circ_2$	2304.8307
43391.627	28	9.0	18		4	0.5		$(^2P^\circ)3p\ ^3P_0$	$(^2P^\circ)3d\ ^3D^\circ_1$	2303.8828
43866.3539	8.5	5.5	5.5		6	1.0		$(^2P^\circ)3p\ ^1P_1$	$(^2P^\circ)3d\ ^1D^\circ_2$	2278.9477
43969.86335	0.76	0.32	0.49	$<10^{-2}$	12	2.2	< 153	$(^2D^\circ)3p\ ^1F_3$	$(^2D^\circ)3d\ ^1G^\circ_4$	2273.5824
44115.3723	2.0	1.7	1.7	−5.1	6	1.5	< 422	$(^2D^\circ)3p\ ^3F_2$	$(^2D^\circ)3d\ ^3F^\circ_2$	2266.0826
44119.1253	1.8	18	18	−14	2	0.5		$(^2D^\circ)3p\ ^3F_4$	$(^2D^\circ)3d\ ^3F^\circ_3$	2265.8898
44139.6792	1.6	1.3	1.6	−1.0	11	1.5	< 417	$(^2D^\circ)3p\ ^3F_3$	$(^2D^\circ)3d\ ^3F^\circ_3$	2264.8346
44155.1346	1.8	43	43	39	1	0.3		$(^2D^\circ)3p\ ^3F_2$	$(^2D^\circ)3d\ ^3F^\circ_3$	2264.0417
44172.2046	1.1	0.85	1.4	−0.1	12	1.7	< 251	$(^2D^\circ)3p\ ^3F_4$	$(^2D^\circ)3d\ ^3F^\circ_4$	2263.1667
44192.7586	1.4	15	15	28	2	0.5		$(^2D^\circ)3p\ ^3F_3$	$(^2D^\circ)3d\ ^3F^\circ_4$	2262.1140
45111.48643	0.72	0.47	0.47		12	2.0	< 205	$(^2D^\circ)3p\ ^3F_4$	$(^2D^\circ)3d\ ^3G^\circ_5$	2216.0400
45138.2549	2.2	11	28	4	4	0.5		$(^2D^\circ)3p\ ^3F_4$	$(^2D^\circ)3d\ ^3G^\circ_4$	2214.7257
45158.8088	1.9	0.55	1.2	$<10^{-2}$	11	2.0	< 230	$(^2D^\circ)3p\ ^3F_3$	$(^2D^\circ)3d\ ^3G^\circ_4$	2213.7176
45182.0312	2.1	8.8	12	−9	5	0.7		$(^2D^\circ)3p\ ^3F_3$	$(^2D^\circ)3d\ ^3G^\circ_3$	2212.5797
45197.4866	1.8	0.68	1.2	0.1	11	1.8	< 265	$(^2D^\circ)3p\ ^3F_2$	$(^2D^\circ)3d\ ^3G^\circ_3$	2211.8230
45248.7942	1.1	0.57	0.73		11	1.9	< 232	$(^2P^\circ)3p\ ^3D_3$	$(^2P^\circ)3d\ ^3F^\circ_4$	2209.3148
45291.4538	1.9	0.99	1.2	−0.2	11	1.6	< 319	$(^2P^\circ)3p\ ^3D_2$	$(^2P^\circ)3d\ ^3F^\circ_3$	2207.2336
45318.9161	2.4	10	10	14	5	0.6		$(^2P^\circ)3p\ ^3D_3$	$(^2P^\circ)3d\ ^3F^\circ_3$	2205.8959
45337.4286	2.3	1.5	1.5		11	1.5	< 465	$(^2P^\circ)3p\ ^3D_1$	$(^2P^\circ)3d\ ^3F^\circ_2$	2204.9951
45356.015	16	23	24	−6	2	0.5		$(^2D^\circ)3p\ ^3F_3$	$(^2D^\circ)3d\ ^1G^\circ_4$	2204.0914
45789.5135	1.2	5.2	8.9	−16	6	0.9		$(^2D^\circ)3s\ ^3D^\circ_1$	$(^2D^\circ)3p\ ^3P_2$	2183.2227
45809.64664	0.85	0.41	0.63	−0.51	11	2.1	260	$(^2D^\circ)3s\ ^3D^\circ_2$	$(^2D^\circ)3p\ ^3P_2$	2182.2631
45839.07314	0.62	0.18	0.42	0.27	12	2.8	257	$(^2D^\circ)3s\ ^3D^\circ_3$	$(^2D^\circ)3p\ ^3P_2$	2180.8620
45885.52765	0.91	0.43	0.74	0.10	12	2.1	269	$(^2D^\circ)3s\ ^3D^\circ_1$	$(^2D^\circ)3p\ ^3P_1$	2178.6539
45905.66078	0.75	0.22	0.55	−0.05	12	2.5	252	$(^2D^\circ)3s\ ^3D^\circ_2$	$(^2D^\circ)3p\ ^3P_1$	2177.6983
45928.2029	1.1	0.35	0.74		12	2.2	248	$(^2D^\circ)3s\ ^3D^\circ_1$	$(^2D^\circ)3p\ ^3P_0$	2176.6293
46201.8910	1.4	0.59	0.94		11	2.0	< 253	$(^4S^\circ)3p\ ^5P_3$	$(^4S^\circ)3d\ ^5D^\circ_4$	2163.7342
46204.5222	2.0	1.8	1.9	−0.7	12	1.5	< 464	$(^4S^\circ)3p\ ^5P_3$	$(^4S^\circ)3d\ ^5D^\circ_3$	2163.6109
46208.0800	2.4	17	37	85	3	0.6		$(^4S^\circ)3p\ ^5P_3$	$(^4S^\circ)3d\ ^5D^\circ_2$	2163.4443
46257.4719	2.0	0.99	1.8	0.6	12	1.8	< 319	$(^4S^\circ)3p\ ^5P_2$	$(^4S^\circ)3d\ ^5D^\circ_3$	2161.1340
46261.0297	2.3	1.6	1.6	0.3	12	1.5	< 458	$(^4S^\circ)3p\ ^5P_2$	$(^4S^\circ)3d\ ^5D^\circ_2$	2160.9678
46264.1173	3.1	6.7	6.7	1.4	5	1.0		$(^4S^\circ)3p\ ^5P_2$	$(^4S^\circ)3d\ ^5D^\circ_1$	2160.8236
46292.1344	2.4	2.8	4.2	−2.9	8	1.3		$(^4S^\circ)3p\ ^5P_1$	$(^4S^\circ)3d\ ^5D^\circ_2$	2159.5156
46295.2220	3.0	2.0	2.0	−0.1	11	1.4		$(^4S^\circ)3p\ ^5P_1$	$(^4S^\circ)3d\ ^5D^\circ_1$	2159.3716
46296.9725	7.2	4.7	4.7		9	1.1		$(^4S^\circ)3p\ ^5P_1$	$(^4S^\circ)3d\ ^5D^\circ_0$	2159.2900
46430.4707	1.8	6.3	6.3	−8.8	6	0.8		$(^2D^\circ)3p\ ^3D_3$	$(^2D^\circ)3d\ ^3F^\circ_3$	2153.0808
46460.0661	2.2	6.1	6.9	−15	6	0.9		$(^2D^\circ)3p\ ^3D_2$	$(^2D^\circ)3d\ ^3F^\circ_2$	2151.7091
46471.0546	2.0	1.1	2.0	8.8	12	1.6	< 383	$(^2D^\circ)3p\ ^3D_1$	$(^2D^\circ)3d\ ^3F^\circ_2$	2151.2003
46483.5500	1.0	0.64	0.78	−0.04	12	1.9	< 283	$(^2D^\circ)3p\ ^3D_3$	$(^2D^\circ)3d\ ^3F^\circ_4$	2150.6220
46499.8284	1.5	0.86	1.3	1.1	12	1.7	< 284	$(^2D^\circ)3p\ ^3D_2$	$(^2D^\circ)3d\ ^3F^\circ_3$	2149.8690
47620.9782	7.4	3.4	4.8		10	1.1		$(^2D^\circ)3p\ ^1P_1$	$(^2D^\circ)3d\ ^1S^\circ_0$	2099.2484
47707.213	14	10	12	−5	6	0.6		$(^2D^\circ)3p\ ^3D_3$	$(^2D^\circ)3d\ ^3D^\circ_3$	2095.4533
47846.266	42	23	27		3	0.6		$(^2D^\circ)3p\ ^3D_2$	$(^2D^\circ)3d\ ^3D^\circ_2$	2089.3627
48085.429	99	64	64		2	0.3		$(^2D^\circ)3p\ ^1F_3$	$(^2D^\circ)3d\ ^1F^\circ_3$	2078.9695
48403.42742	0.61	0.21	0.39	$<10^{-3}$	12	2.7	335	$(^2D^\circ)3s\ ^1D^\circ_2$	$(^2D^\circ)3p\ ^1D_2$	2065.3094
48569.126	10	30	30	43	2	0.5		$(^2P^\circ)3p\ ^3S_1$	$(^2P^\circ)3d\ ^3P^\circ_2$	2058.2625
53185.609	23	15	15		4	0.7		$(^2P^\circ)3s\ ^1P^\circ_1$	$(^2P^\circ)3p\ ^1S_0$	1880.2079

[a]Ritz wavenumbers and uncertainties for ^{20}Ne derived with error-correction factor $k_1 = 1.53$. [b]One standard deviation uncertainties, given with two significant digits to make the steps in the analysis possible to follow. [c]Number of lines used to calculate σ_ϵ. [d]Lowest intensity of the lines used to calculate σ_ϵ. [e]In units of cm^{-1}. Also includes estimated conservative upper limits to transitions without visible IS. [f]Air wavelengths above 2000 Å, calculated with refractive index of air from [23], vacuum wavelengths below 2000 Å.

lines and the investigated lines are from singly-ionized noble gases. Under the same pressure and current, there were no systematic shifts in wavenumber between the calibrated lines from the discharge inside a 6 and a 9 mm HC bore, which is expected if there are illumination shifts present.

5.3 Energy levels

The purpose of this work is to give accurate Ritz wavenumbers in the region 2000 to 5000 Å, i.e. only the relative positions of the energy levels involved in the observed transitions are important. If the number of resonance lines needed to define the level system is minimized, there will be no influence on the Ritz wavenumbers from these transitions. Therefore, to fix the energy level system of Ne II to the ground state, only two of the resonance transitions used in [5] were employed here. The $2s2p^6$ $^2S_{1/2}$ level is the lowest involved in transitions observed in this work, which is connected to the $2s^22p^5$ $^2P^\circ$ ground term by the 216267.28 (0.14) and 217047.61 (0.14) cm^{-1} resonance transitions measured by Persson [21]. The fine-structure splitting of the ground term has been determined to be 780.4240 (0.0011) cm^{-1} [25]. By the 37117.3992 (0.0013) cm^{-1} transition measured in this work, $2s2p^6$ $^2S_{1/2}$ is connected to $2s^22p^4(^3P)3p$ $^2P^\circ_{3/2}$, which is the level involved in the greatest number of observed transitions.

After a weighted fit, including the transitions above, the energy-level uncertainties were dominated by the contribution from the resonance transitions. To make the values of the uncertainties in Table 5 more transparent, the uncertainty of $(^3P)3p$ $^2P^\circ_{3/2}$ was subtracted in quadrature from all levels that were not involved in the resonance transitions. Even though the observed wavenumbers in this work are the line centers positions of ^{20}Ne, the level energies in Table 5 do not correspond to those of ^{20}Ne, since the transition isotope shifts of the Ne II resonance transitions from [21] are unknown, preventing a derivation of the level isotope shifts. However, when taken relative to each other, all $2s^22p^4nl$ levels where $n > 2$ have energies that correspond to those of ^{20}Ne. Individually the two resonance transitions give an energy of the $2s2p^6$ $^2S_{1/2}$ level that is well within the confidence interval of the energy given in Table 5. This shows that the contributions from IS to corresponding wavenumbers in [21] differ less than the uncertainties involved.

The choice of previously measured resonance transitions to make the Ne III system non-singular is not as obvious as for Ne II. Instead, this was achieved by dividing the least-squares fitting of the levels into three independent systems of equations, with the lowest level in each of them fixed. In Equation (2) this is done by simply adding a virtual transition to y with the same wavenumber as the energy of the fixed level and then modifying A to include it as a resonance transition. An uncertainty of this wavenumber must be assumed, which, after solving the system, is subtracted from the uncertainties of the connected level energies, thereby, making them relative to the fixed level.

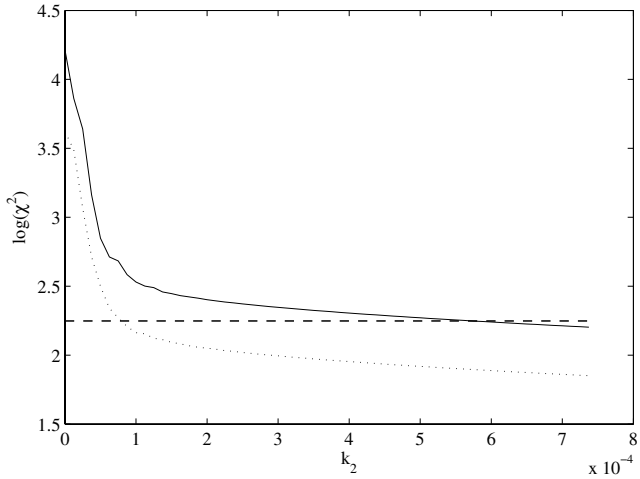

Fig. 6. Logarithm of χ^2 defined by equation (5) versus error-correction factor k_2 for Ne II. Solid line has a k_1 of 0 and dotted 1.53. The degrees of freedom are shown as a dashed line, which equals χ^2 for the non-zero k_1 at $k_2 = 7.5 \times 10^{-5}$.

The three systems of equations are fitted simultaneously to make it possible to derive a global value of the error correction k_1. In this work the $2s^22p^3(^4S)3s$ $^5S^\circ_2$, $(^4S)3s$ $^3S^\circ_1$ and $(^2D)3s$ $^3D^\circ_3$ levels were fixed at the energies derived in [6], see Table 6. The level energies in Table 6 do not correspond to those of ^{20}Ne, since the level isotope shifts of the fixed levels are unknown and have not been taken into account. However, within each group of levels with energies derived from the same fixed level, i.e. sharing the same superscript in Table 6, the relative level energies correspond to those of ^{20}Ne.

When fitting the observed Ne III transitions to the level system, a moderate k_1 of 1.53 had to be used in the error matrix (3). For Ne II, using only the multiplicative factor k_1, a value larger than 6.9 was needed. On the other hand, with a non-zero k_2 only, a value of about 0.00058 cm^{-1} had to be used to correct χ^2. If either of these are employed, many transitions will have severely overestimated uncertainties. From Figure 6 it is obvious that the main contributors to the large k_1 are the transitions with the lowest uncertainties, while the large k_2 is explained by the large difference in size of the uncertainties. Adopting a k_1 of 1.53 for Ne II, the same as for Ne III, a k_2 of 7.5×10^{-5} cm^{-1} is needed, which is of the same order of magnitude as the lowest uncertainties u_ϵ of the strongest transitions. These values of k_1 and k_2 were used in the analysis of Ne II.

Ritz wavenumbers σ_{Ritz} were calculated from the fitted level energies and corresponding uncertainties u_{Ritz} were derived from the covariance matrix of (4). By the nature of the analysis the values of σ_{Ritz}, presented in Tables 3 and 4, correspond to transitions in ^{20}Ne. Some σ_{Ritz} have uncertainties as low as 0.0001 cm^{-1}, which is half of the stated uncertainty of the most accurate Ar II reference wavenumbers in [7]. Most transitions have values of $\sigma_{Ritz} - \sigma_\epsilon$ that are less than two u_ϵ, which shows that the internal consistency of the data is strong even prior to

Table 5. Fitted energy levels in Ne II.

Config.[a]	Term	J	Energy[b] (cm^{-1})	$u(E)$ (10^{-3})	lines[c]	Config.[a]	Term	J	Energy[b] (cm^{-1})	$u(E)$ (10^{-3})	lines[c]
$2s^22p^5$	$^2P^\circ$	3/2	0	0	2	(^3P)3d	^2D	5/2	280269.01270	0.13	7
		1/2	780.4240	1.1	2			3/2	280473.62429	0.15	10
$2s2p^6$	^2S	1/2	217047.66	100	4	(^3P)3d	^4P	1/2	280768.5756	0.3	5
(^3P)3s	^4P	5/2	219130.82934	0.13	8			3/2	280989.5903	0.2	10
		3/2	219648.49372	0.12	9			5/2	281171.42446	0.12	9
		1/2	219947.51257	0.13	7	(^3P)3d	^2P	1/2	281332.5889	0.3	6
(^3P)3s	^2P	3/2	224087.07540	0.08	8			3/2	281720.34204	0.13	7
		1/2	224699.33911	0.09	7	(^3P)4s	^4P	5/2	281998.3332	0.2	6
(^3P)3p	$^4P^\circ$	5/2	246192.47965	0.14	15			3/2	282375.3740	0.2	8
		3/2	246415.08068	0.13	15			1/2	282680.6976	0.3	5
		1/2	246597.74784	0.15	11	(^3P)4s	^2P	3/2	283322.39835	0.11	7
(^1D)3s	^2D	5/2	246394.1880	0.6	8			1/2	283894.46327	0.14	4
		3/2	246397.5490	0.6	9	(^3P)4p	$^2D^\circ$	5/2	292033.198	12	1
(^3P)3p	$^4D^\circ$	7/2	249108.68107	0.15	10			3/2	292451.828	6	2
		5/2	249446.02987	0.12	16	(^3P)4p	$^2S^\circ$	1/2	292546.763	9	1
		3/2	249695.57196	0.13	17	(^3P)4p	$^2P^\circ$	3/2	294086.5292	1.0	2
		1/2	249839.68482	0.15	9			1/2	294333.2577	1.0	1
(^3P)3p	$^2D^\circ$	5/2	251011.21801	0.10	13	(^1D)3d	^2G	9/2	305364.0744	0.6	1
		3/2	251522.16394	0.10	14			7/2	305365.1844	0.6	2
(^3P)3p	$^2S^\circ$	1/2	252798.53091	0.10	10	(^1S)3p	$^2P^\circ$	3/2	305398.6656	5	2
(^3P)3p	$^4S^\circ$	3/2	252953.58536	0.13	18			1/2	305408.5577	5	2
(^3P)3p	$^2P^\circ$	3/2	254165.05568[d]	100 (0)	22	(^1D)3d	^2P	3/2	305566.9888	0.6	5
		1/2	254292.23597	0.10	14			1/2	305582.3159	0.7	4
(^1D)3p	$^2F^\circ$	5/2	274364.6266	0.6	7	(^1D)3d	^2S	1/2	306011.1224	0.6	4
		7/2	274409.1510	0.6	6	(^1D)3d	^2D	5/2	306243.4750	0.6	5
(^1D)3p	$^2P^\circ$	3/2	276276.9002	0.6	11			3/2	306262.8212	0.6	6
		1/2	276511.8636	0.6	8	(^1D)3d	^2F	5/2	306687.3402	0.6	3
(^1S)3s	^2S	1/2	276677.184	5	5			7/2	306687.7256	0.6	2
(^1D)3p	$^2D^\circ$	3/2	277325.6422	0.6	9	(^3P)5p	$^4D^\circ$	3/2	307774.759	6	1
		5/2	277344.3345	0.6	9	(^3P)5p	$^2S^\circ$	1/2	308006.934	11	1
(^3P)3d	^4D	7/2	279137.67332	0.15	4	(^1D)4s	^2D	5/2	308101.3139	0.6	5
		5/2	279218.7103	0.2	6			3/2	308101.6730	0.6	5
		3/2	279324.9419	0.2	7	(^3P)5p	$^4S^\circ$	3/2	308136.937	10	1
		1/2	279422.9374	0.3	5	(^3P)5p	$^2D^\circ$	3/2	308177.250	7	1
(^3P)3d	^4F	9/2	280173.0559	0.2	1	(^3P)5p	$^2P^\circ$	3/2	308738.078	5	1
		7/2	280700.81296	0.13	4			1/2	308976.903	5	1
		5/2	280797.30713	0.14	8	(^1D)4p	$^2P^\circ$	3/2	317663.175	7	1
		3/2	280947.1445	0.2	9			1/2	317828.380	15	1
(^3P)3d	^2F	7/2	280262.38414	0.14	3	(^1S)4s	^2S	1/2	338788.816	7	2
		5/2	281026.00165	0.14	9						

[a]Level assignment of [21]. [b]Absolute level energies do not correspond to a specific isotope. However, for all $2s^22p^4nl$ levels where $n > 2$ the differences in energies between them correspond to those of ^{20}Ne, see Section 5.3 for details. [c]Number of observed transitions connected to the level. [d]All other uncertainties in the $2s^22p^4nl$ configurations where $n > 2$ are relative to this level.

the level fitting. The consistency is further strengthened by the non-zero k_1 and k_2.

Clearly, a relatively large error is present in the Ne II transitions with the lowest uncertainties. Even though only low current spectra are used for these, a probable strong contributor to the non-zero k_2 are Stark shifts. Further, the other errors discussed in Section 5.2 will also have an effect. For Ne III k_2 has no influence due to the lower S/N of these lines. The non-random noise, discussed in Section 4.4, has been compensated for with a k_1 of 1.53. There are also other omitted covariances that can contribute to k_1. After calibration, the line positions measured in a spectrum are no longer statistically independent. Further, the Ar II reference wavenumbers are considered independent of each other, which may not be the case.

Also, line profiles without noticeable structure, i.e. 3p–3d and 3p–4s transitions, are still asymmetric due to the three isotope components. Even if not showing any trace in the residuals when fitting a symmetrical function, this may influence the line center positions. These were assumed to correspond to the position of the ^{20}Ne component and will, therefore, contribute to errors that affect the values of k_1 and k_2.

Table 6. Fitted energy levels of Ne III.

Config.[a]	Term	J	Energy[b] (cm^{-1})	$u(E)$ (10^{-3})	lines[c]	Config.[a]	Term	J	Energy[b] (cm^{-1})	$u(E)$ (10^{-3})	lines[c]
$2s^22p^4$	^3P	2	0.0[d]	0		$(^2D^\circ)3p$	^3P	2	398972.6781[g]	0.6	6
		1	642.872[d]	13				1	399068.6922[g]	1.2	6
		0	920.550[d]	13				0	399111.3675[g]	1.5	1
$2s^22p^4$	^1D	2	25840.72[d]	200		$(^2D^\circ)3p$	^1D	2	406332.439[g]	15	2
$2s^22p^4$	^1S	0	55752.7[d]	900		$(^2P^\circ)3p$	^3S	1	409873.286[g]	6	4
$2s2p^5$	$^3P^\circ$	2	204290.0[d]	1100		$(^2P^\circ)3p$	^3D	3	412348.004[g]	5	3
		1	204872.6[d]	1100				2	412375.466[g]	5	3
		0	205194[d]	2000				1	412376.477[g]	8	3
$2s2p^5$	$^1P^\circ$	1	289478.6[d]	1000		$(^2P^\circ)3p$	^1P	1	414229.160[g]	15	2
$(^4S^\circ)3s$	$^5S^\circ$	2	309881.0410[d,e]	2000 (0)	4	$(^2P^\circ)3p$	^3P	0	416723.403[g]	7	2
$(^4S^\circ)3s$	$^3S^\circ$	1	319431.2610[d,f]	900 (0)	4			1	416753.018[g]	5	6
$(^4S^\circ)3p$	^5P	1	348395.5159[e]	0.6	4			2	416798.035[g]	5	6
		2	348426.6207[e]	0.5	4	$(^2P^\circ)3p$	^1D	2	420244.570[g]	15	2
		3	348479.5704[e]	0.5	4	$(^2P^\circ)3p$	^1S	0	433012.00[g]	30	1
$(^2D^\circ)3s$	$^3D^\circ$	3	353133.6050[d,g]	50 (0)	6	$(^2D^\circ)3d$	$^3F^\circ$	2	435515.616[g]	2	3
		2	353163.0315[g]	1.0	8			3	435555.378[g]	2	5
		1	353183.1646[g]	1.3	7			4	435608.4575[g]	1.0	3
$(^4S^\circ)3p$	^3P	1	356751.8341[f]	0.3	3	$(^2D^\circ)3d$	$^1S^\circ$	0	435583.15[g]	20	1
		0	356761.866[f]	3	2	$(^2D^\circ)3d$	$^3G^\circ$	5	436547.7393[g]	0.8	1
		2	356762.7936[f]	0.7	3			4	436574.508[g]	2	2
$(^2D^\circ)3s$	$^1D^\circ$	2	357929.011[g]	15	3			3	436597.730[g]	2	2
$(^2P^\circ)3s$	$^3P^\circ$	1	374489.468[g]	5	7	$(^2D^\circ)3d$	$^1G^\circ$	4	436771.714[g]	15	2
		0	374490.122[g]	6	3	$(^2D^\circ)3d$	$^3D^\circ$	3	436832.120[g]	14	2
		2	374496.030[g]	5	5			2	436901.82[g]	40	1
$(^2P^\circ)3s$	$^1P^\circ$	1	379826.387[g]	15	4	$(^2D^\circ)3d$	$^3P^\circ$	2	439573.020[g]	11	1
$(^2D^\circ)3p$	^1P	1	387962.168[g]	15	3			1	439694.77[g]	40	2
$(^2D^\circ)3p$	^3D	1	389044.5613[g]	1.4	3			0	439747.743[g]	15	1
		2	389055.5498[g]	1.0	6	$(^2D^\circ)3d$	$^3S^\circ$	1	440051.618[g]	3	1
		3	389124.9076[g]	0.3	5	$(^2D^\circ)3d$	$^1F^\circ$	3	440887.28[g]	100	1
$(^2D^\circ)3p$	^3F	2	391400.2436[g]	1.3	5	$(^2P^\circ)3d$	$^3F^\circ$	4	457596.798[g]	5	1
		3	391415.6989[g]	1.0	7			3	457666.920[g]	6	2
		4	391436.2529[g]	0.4	5			2	457713.906[g]	9	1
$(^2D^\circ)3p$	^1F	3	392801.851[g]	15	4	$(^2P^\circ)3d$	$^1D^\circ$	2	458095.51[g]	20	1
$(^4S^\circ)3d$	$^5D^\circ$	4	394681.4613[e]	1.5	1	$(^2P^\circ)3d$	$^3P^\circ$	0	458286.300[g]	13	1
		3	394684.093[e]	2	2			1	458335.37[g]	40	1
		2	394687.650[e]	2	3			2	458442.412[g]	11	3
		1	394690.738[e]	3	2	$(^2P^\circ)3d$	$^3D^\circ$	1	460115.03[g]	30	1
		0	394692.488[e]	7	1			2	460126.801[g]	13	2
$(^4S^\circ)3d$	$^3D^\circ$	1	398178.082[f]	12	2			3	460138.777[g]	10	1
		2	398182.795[f]	4	2	$(^2P^\circ)3d$	$^1F^\circ$	3	460120.00[g]	20	1
		3	398195.515[f]	3	1						

[a]Level assignment of [6]. [b]Absolute level energies do not correspond to a specific isotope. However, within each group, as specified by superscripts e, f and g, the differences in energies between levels correspond to those of ^{20}Ne, see Section 5.3 for details. [c]Number of observed transitions connected to the level. [d]Energies and uncertainties taken from [6]. [e]Energy and uncertainty relative to $2s^22p^3(^4S^\circ)3s\ ^5S^\circ_2$. [f]Energy and uncertainty relative to $2s^22p^3(^4S^\circ)3s\ ^3S^\circ_1$. [g]Energy and uncertainty relative to $2s^22p^3(^2D^\circ)3s\ ^3D^\circ_3$.

The wavenumbers of Ne II derived in this work were compared with corresponding Ritz wavelengths in [5], which were converted to air wavelengths by the five-parameter dispersion formula suggested in [26]. To minimize errors in the comparison, the same formula was used here. From Figure 7 it is clear that there are systematic differences. The wavenumbers for the 3s–3p transitions tend to be higher in [5] than in present work, while those for the 3p–3d and 3p–4s transitions are lower.

For most of the transitions in Figure 7, the Ne II Ritz wavelengths in [5] were derived from the observed wavenumbers in [27]. It was concluded in [27] that the given wavenumbers of a number of Ne I 3s–3p transitions were blue shifted 0.003 cm^{-1} from the position of the ^{20}Ne isotope. The IS of Ne I 3s–3p transitions have values of about 0.05 cm^{-1} and have the same sign as those of Ne II 3s–3p transitions, see e.g. [28]. Therefore, Ritz wavelengths in [5], with corresponding observed wavenumbers

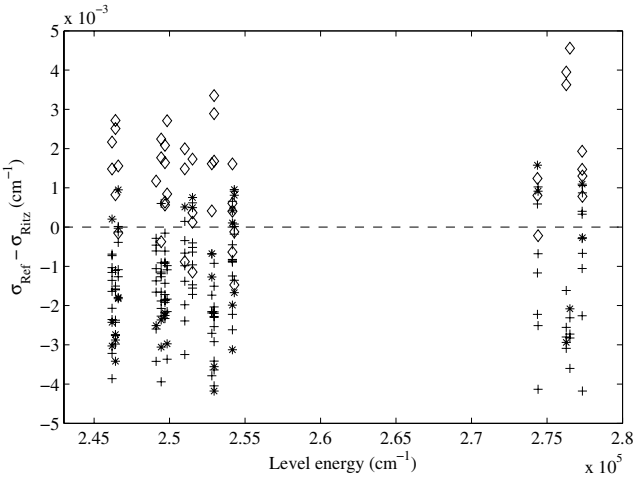

Fig. 7. Difference between Ritz wavenumbers derived in this work (σ_{Ritz}) and those of [5] (σ_{Ref}), plotted versus the energy of the 3p levels involved in the transitions. Here, 3s–3p transitions are shown as diamonds, 3p–3d as crosses and 3p–4s as stars. Corresponding wavenumbers in [5] have uncertainties about 0.0015, 0.002 and 0.0015 cm^{-1}, while in present work the uncertainties are an order of magnitude lower. The mean of the shifts are 0.0013, −0.0012 and −0.0013 cm^{-1}, respectively.

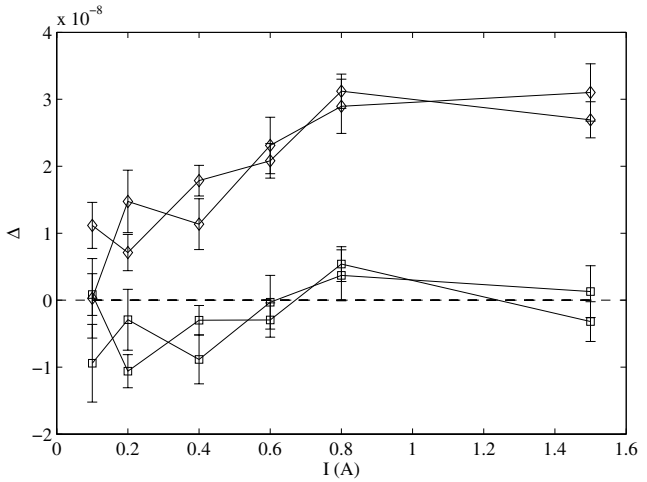

Fig. 8. Δ as a function of current at a constant pressure of 0.25 torr, formed by 3d–4p and 4s–4p Ar II calibration lines, see equation (13). The lines correspond to Δ(21996/22716) and Δ(23644/24907) (diamonds); and Δ(21996/23644) and Δ(22716/24907) (squares). Error bars do not take the uncertainty of σ_{corr} into account, since only the change is of importance.

taken from [27], must be blue shifted from the ^{20}Ne isotope position. The Ritz wavenumbers derived in the present work correspond to transitions in ^{20}Ne, which explains the systematic blue shifts of the 3s–3p transitions in Figure 7. The red shift of the 3p–3d and 3p–4s transitions is probably due to calibration errors in [27]. If this is the case, the 3s–3p transitions have been red shifted by the same amount, which has reduced the apparent blue shift of these transitions. The bulk of the shifts in Figure 7 fall within the stated uncertainties in [5]. These are, however, an order of magnitude larger than in the present work.

When comparing Ne III wavenumbers derived in this work with the Ritz wavelengths in [6], the 3s–3p transitions tend to be blue shifted in the latter. In [6] the observed wavenumbers of these transitions were determined by fitting a Voigt function to the line profiles in FTS spectra from a HC. This gives a value somewhere between the position of the ^{20}Ne isotope and the center of gravity of the profile, which explains the tendency towards blue shifted Ritz wavelengths in [6]. Most of the observed wavenumbers of the 3p–3d transitions in [6] were taken from [22] and corresponding Ritz wavelengths show no systematic shifts. The main part of the shifts from the wavenumbers in the present work fall within the uncertainties of [6]. Corresponding uncertainties in Table 4 are, however, an order of magnitude smaller.

6 Stark shifts

The Doppler widths of the observed line profiles increase with current, with corresponding ion temperatures ranging from 400 to 700 K. However, if PLTE is assumed for levels involved in UV–VIS transitions, typical excitation temperatures in a DC HC discharge plasma are between 10000 and 30000 K for singly-ionized buffer gas atoms, see e.g. [13]. A well-known limitation to the PLTE assumption is the fact that the electron energy in a DC HC plasma does not show a Maxwellian distribution. Another limitation is that typical electron densities in a DC HC plasma are of the order 10^{13} cm^{-3} [29].

With the Ar II calibration lines produced in the same plasma as the neon lines, there is no direct method to derive absolute values of a Stark shift. However, there is a simple method to detect its presence. If not affected by shifts, the ratio between wavenumbers of two lines in the same spectrum is independent of the calibration (12), i.e.

$$\Delta(a/b) = \frac{\sigma_{obs,a}}{\sigma_{obs,b}} - \frac{\sigma_{corr,a}}{\sigma_{corr,b}}, \qquad (13)$$

where Δ is equal to zero. Here, σ_{corr} are the reference wavenumbers of [7], which are assumed to be unaffected by Stark shifts. If shifts are present, this can result in a Δ deviating from zero, especially if only one line is shifted or both, but in opposite directions. Stark shifts in Ar II have been investigated in [30] at excitation temperature similar to those in a DC HC plasma, but electron densities several orders of magnitude larger. From the data presented in [30], it is clear that 4s–4p transitions are blue shifted, while the 3d–4p transitions are red shifted.

Six HC spectra were recorded at a pressure of 0.25 torr, but with the current increased in sequence from 0.10 to 1.50 A. The 21996 and 23644 cm^{-1} 4s–4p transitions in conjunction with the 24907 and 22716 cm^{-1} 3d–4p transitions, prominent Ar II calibration lines, were used to form the ratios in (13). A clear increase of Δ(4s–4p/3d–4p) with the current was found, see Figure 8. A probable explanation to this behavior is blue shifted 4s–4p transitions and red shifted 3d–4p transitions, the same as reported in [30].

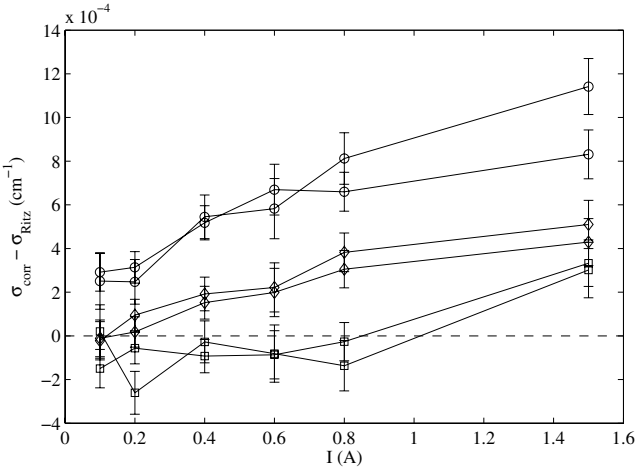

Fig. 9. Shift from σ_{Ritz} of strong Ne II 3s–3p transitions relative to Ar II standards, plotted as a function of current. The transitions are among the strongest in the ^{4}P–^{4}P° (squares), ^{2}D–(^{1}D)^{2}P° (diamonds) and ^{2}D–^{2}F° (circles) multiplets. Error bars do not take the uncertainty of σ_{Ritz} into account, since only the change is of importance.

Assuming only one of the transitions is influenced by the Stark effect, the Δ at 0.40 A corresponds to a maximum shift of 0.0004 cm^{-1}. At low currents Δ approaches zero, indicating a smaller effect on the Ar II calibration lines.

From Figure 8 it can also be concluded that the current dependence does not arise from Doppler shifts due to motions in the discharge plasma. If this were the case, the Δ(4s–4p/4s–4p) and Δ(3d–4p/3d–4p) would have the strongest dependence, since the wavenumber differences of the transitions in these Δ are greater than in Δ(4s–4p/3d–4p). Also, no dependence on the buffer gas pressure was found.

After calibrating a spectrum with Ar II standards, all measured shifts of the neon lines are relative to the bulk of the argon lines, which in turn may be Stark shifted. In Figure 9, Ritz wavenumbers of strong Ne II 3s–3p transitions are subtracted from calibrated wavenumbers measured in the current sequence described above. Clearly, the ^{4}P–^{4}P° multiplet has the smallest shifts, while ^{2}D–^{2}F° has the largest. For higher currents, the separation between these two multiplets is as large as 0.0006 cm^{-1}, setting a lower limit to a true Stark shift of 0.0003 cm^{-1} for one of them. The multiplets not depicted have blue shifts somewhere between ^{2}D–(^{1}D)^{2}P° and ^{2}D–^{2}F°. Blue shifted Ne II 3s–3p transitions have also been observed in [1] at similar excitation temperatures but higher electron densities. The direction of a Stark shift can depend on these two parameters and a strict comparison is not possible, since they have not been determined in this work. As expected from [31], transitions within a multiplet have shifts following the same current dependence. That the shifts approach zero at low currents confirms that the Stark effect has been minimized in the σ_{Ritz} presented in Table 3.

To test the Ne II 3s–3p transitions as tertiary wavenumber standards, spectra were calibrated both with these and the Ar II secondary standards, see Table 7. To compensate for the reduced χ^2_ϵ deviating from unity when calculating the mean of α by equation (8), an ϵ was added in quadrature to the uncertainties of the wavenumbers. At low currents, the reduced χ^2_ϵ of both Ne II and Ar II are close to unity. The values of α are in close agreement and both standards can be used with confidence. When the current is increased, the two standards diverge and a significant ϵ has to be introduced for both elements. With the higher uncertainties of both argon measurements and standards, the lower ϵ of neon shows a stronger internal consistency of the Ne II lines. Either they are less affected by Stark shifts, or they are all shifted in the same direction. Assuming only one of the elements is affected, the difference in α at higher currents gives shifts of about 0.0005 cm^{-1} for a 30000 cm^{-1} transition, which can be adopted as a local error when calibrating nearby spectral lines.

Spectra from the HC with the smaller 3 mm bore have large reduced χ^2_ϵ, even if recorded at low currents. This can be explained by the smaller plasma volume, which gives a higher electron density. Increasing the bore diameter from 6 to 9 mm has no significant influence on the χ^2_ϵ. Also, a higher pressure has a damping effect on χ^2_ϵ. This may be explained by the decrease in strength of the ionized gas lines, but also in a reduced Stark effect.

The Lorentzian width $\delta\sigma_L$ of the line profiles is a sum of natural and Stark broadening. The former is an intrinsic property due to the finite lifetimes of the levels involved in the transition, see e.g. [32], while the latter is assumed to be caused by free electrons in the discharge plasma, since the width is unaffected by changes in pressure but increases linearly with the current. The currents in this investigation were in the range 0.05 to 1.50 A. Natural widths $\delta\sigma_n$ for the 3s–3p transitions in Ne II were calculated using the semi empirical A-values in [33], from which it was evident that they can contribute significantly to the observed Lorentzian widths. As an example, transitions within the 3s ^{4}P–3p ^{4}P° multiplet have a $\delta\sigma_n$ of 0.0007 cm^{-1} and $\delta\sigma_L$ increase linearly from 0.005 to 0.060 cm^{-1} with the current, while those within 3s ^{2}D–(^{1}D)3p ^{2}P° have a $\delta\sigma_n$ of 0.011 cm^{-1} and $\delta\sigma_L$ increase from 0.013 to 0.015 cm^{-1}. The 3s ^{4}P levels have lifetimes above 100 ns, while for the 3s ^{2}D levels they are below 1 ns. From this and the fact that Lorentzian widths of the ^{4}P–^{4}P° multiplet are more sensitive to current changes than those of the ^{2}D–^{2}P° multiplet, it can be concluded that the driving mechanism is not resonance broadening, since this is proportional to the transition probability of the resonance transitions from the 3s levels, see e.g. [32]. The values of $\delta\sigma_L$ are sensitive to self-absorption of the spectral lines and may have been overestimated above. However, in contrast to the Lorentzian widths, no clear current dependence was found for the self-absorption, see Section 3.

7 Conclusions

The 3s–3p transitions of Ne II presented in this work are recommended as tertiary wavelength standards for high

Table 7. Calibration factor α for 9 region **A** spectra calculated with both Ar II standards and Ne II 3s–3p transitions. The wavenumbers used to calculate α for each element have uncertainties of the same magnitude. Due to possible blends a number of Ar II transitions were removed at higher currents.

Spectrum	Element	N_f^a	χ^2_ϵ / N_f	α^b_{wm}	$u(\alpha_{wm})^b$	α^b_ϵ	$u(\alpha_\epsilon)^b$	ϵ (10^{-3} cm^{-1})	I (A)	P^c_{part} (torr)
1	Ne	24	1.21	1025.4	1.0	1025.6	1.2	0.07	0.05	0.39
	Ar	24	1.34	1026.2	2.0	1025.9	2.4	0.15		0.10
2	Ne	24	1.07	1035.5	1.1	1035.6	1.1	0.04	0.05	0.60
	Ar	24	1.19	1037.9	2.1	1037.7	2.4	0.12		0.15
3	Ne	24	1.43	917.3	0.8	917.4	1.0	0.07	0.10	0.20
	Ar	24	1.46	920.4	2.1	919.9	2.7	0.19		0.05
4	Ne	24	2.72	926.6	0.8	927.0	1.2	0.14	0.20	0.20
	Ar	22	1.46	929.2	2.1	928.7	2.7	0.17		0.05
5	Ne	24	3.43	946.4	0.8	946.7	1.3	0.15	0.40	0.20
	Ar	22	2.89	957.1	2.1	956.3	3.6	0.33		0.05
6	Ne	24	4.20	823.2	0.8	823.9	1.5	0.19	0.60	0.20
	Ar	22	7.86	837.2	2.2	833.5	6.4	0.68		0.05
7	Ne	24	4.55	838.0	0.8	838.5	1.6	0.20	0.80	0.20
	Ar	22	7.05	856.1	2.1	853.5	5.9	0.61		0.05
8	Ne	24	3.56	1008.1	0.8	1008.5	1.5	0.18	1.50	0.20
	Ar	21	1.81	1031.1	2.2	1030.3	3.3	0.25		0.05
9	Ne^d	24	52.5	980.5	0.9	984.2	6.3	0.90	0.05	0.08
	Ar^d	22	5.56	989.8	2.0	989.6	5.1	0.52		0.02

[a]Degrees of freedom of the mean, i.e. $n-1$ where n is the number of transitions. [b]Times scale factor of 10^{-9}. [c]Partial pressure. [d]HC bore diameter 3 mm, all others 6 mm.

accuracy measurements. According to [1] these neon transitions are the least sensitive to Stark shifts and when deriving the Ritz wavenumbers in this work, these shifts have been minimized. The resulting uncertainties are about half of what is stated for the Ar II secondary standards [7]. From the point of view of Stark shifts, there is no evidence that Ar II standards are better than the Ne II standards presented here. Individual lines may shift in different direction while the mean shift of all calibration lines is close to zero. However, if only relative line positions are needed, it was shown in Section 6 that the Ne II lines are better, since they show a stronger internal consistency in high current spectra. The Ne II transitions within the 3s ^{4}P–3p ^{4}P° multiplet have the smallest current dependence relative to the bulk of the Ar II standards. These transitions are therefore recommended as standards if the shift relative to the Ar II standards is to be minimized.

Stark shifts have not been observed in the 3p–3d and 3p–4s transitions of Ne II, nor in any of the Ne III transitions, due to the lower S/N of these lines. If the lower uncertainties are adequate, these transitions can also be used as wavenumber standards. However, caution is needed if the line center positions can be determined to a better accuracy than in this work.

In many situations the IS of the 3s–3p transitions can be unresolved, e.g. due to instrumental or thermal broadening of the spectral lines. Instead, the line profiles appear asymmetric. If this is the case, to reach a high accuracy when calibrating a spectrum with these transitions, the position of the ^{20}Ne line center must be determined. This can be done by a deconvolution of line profiles, using a fitting routine similar to those described in Section 4.1. For a good determination of the position, the fitting requires that either the IS or the isotope area ratio is fixed. The IS are known from Tables 1 and 2 in this work, while the area ratio must somehow be determined, which in turn can be affected by self-absorption. The latter is also a reason for avoiding the center of gravity method when determining position of the ^{20}Ne line center. If self-absorption is absent and the relative abundance of the three neon isotopes is known, the ^{21}Ne isotope can readily be included in a center of gravity measurement, since its position is known by equation (1).

If a symmetric profile is used to fit the 3s–3p transitions, the resulting line center positions have large systematic blue shifts from the ^{20}Ne line center positions. To give an example, a pure Voigt function was fitted to these transitions in spectra recorded with a buffer gas pressure of 0.25 torr. Transitions with a ^{2}P lower term will be shifted 0.0005 and 0.001 cm^{-1} at a discharge current of 0.40 and 0.80 A, respectively. Under the same discharge conditions, transitions with a ^{4}P lower term are shifted 0.003 and 0.004 cm^{-1}, which are larger due to the smaller IS of these transitions. The size of the blue shift increases with $\delta\sigma_D/IS$, which in turn introduces a wavelength dependence.

In Section 6 it is shown that the experimental setup in this work can be used to study Stark effects at lower electron densities than what is common in that field. With the double-sided HC used in this work, it is possible to

send light from a second spectral lamp through the HC to the FTS. If the HC is single-sided, the light from the two lamps can instead be combined with a beam splitter. Lines from the second source can then be used as references for absolute values of Stark shifts in the HC plasma. Further, if the number of data points per line profile is increased about an order of magnitude, Stark broadening can simultaneously be studied with great accuracy.

Covariance matrices and energy levels from fitting the observed transitions to the level systems of Ne II and Ne III are published as *Supplementary Online Material*. This enables the reader to calculate Ritz wavenumbers and uncertainties for transitions not included in Tables 3 and 4.

The author would like to thank Prof. Lennart Lindegren for rewarding discussions and ideas regarding the statistics, Prof. Glenn Wahlgren for the support in writing the paper, Dr. Kaj Söderström for the help with the mass-spectrometer measurements and the anonymous referees for improving the manuscript.

References

1. S. Djeniže, V. Milosavljević, M.S. Dimitrijević, Astron. & Astrophys. **382**, 359 (2002)
2. K.J.R. Rosman, P.D.P. Taylor, Pure Appl. Chem. **70**, 217 (1998)
3. K. Murakawa, Phys. Rev. A **11**, 778 (1956)
4. W.C. Kreye, J. Opt. Soc. Am. **64**, 186 (1974)
5. A.E. Kramida, G. Nave, Eur. Phys. J. D **39**, 331 (2006)
6. A.E. Kramida, G. Nave, Eur. Phys. J. D **37**, 1 (2006)
7. W. Whaling, W.H.C. Anderson, M.T. Carle, J.W. Brault, H.A. Zarem, J. Quant. Spectrosc. Radiat. Transfer **53**, 1 (1995)
8. A.P. Thorne, C.J. Harris, I. Wynne-Jones, R.C.M. Learner, G. Cox, J. Phys. E **20**, 54 (1987)
9. J.W. Brault, Mikrochim. Acta **3**, 215 (1987)
10. G. Nave, C.J. Sansonetti, U. Griesmann, Opt. Soc. Am. Tech. Digest Ser. **3**, 38 (1997)
11. R.C.M. Learner, A.P. Thorne, J. Opt. Soc. Am. B **5**, 2045 (1988)
12. *Improved hollow cathode lamps for atomic spectroscopy*, edited by S. Caroli (Ellis Horwood limited, West Sussex, 1985)
13. U. Griesmann, J. Musielok, W.L. Wiese, J. Opt. Soc. Am. B **14**, 2204 (1997)
14. F. Biraben, E. Giacobino, G. Grynberg, Phys. Rev. A **12**, 2444 (1975)
15. W.H. King, *Isotope shifts in atomic spectra* (Plenum Press, New York, 1984)
16. F. Schreier, J. Quant. Spectrosc. Radiat. Transfer **48**, 743 (1992)
17. J. Humlíček, J. Quant. Spectrosc. Radiat. Transfer **27**, 437 (1982)
18. P.R. Bevington, D.K. Robinson, *Data reduction and error analysis for the physical sciences,* 3rd edn. (McGraw-Hill, New York, 2003)
19. L.J. Radziemski, K.J. Fisher, D.W. Steinhaus, A.S. Goldman, Comp. Phys. Commun. **3**, 9 (1972)
20. D.S.G. Pollock, *A handbook of time-series analysis, signal processing and dynamics* (Academic Press, San Diego, 1999)
21. W. Persson, Phys. Scripta **3**, 133 (1971)
22. W. Persson, C.-G. Wahlström, L. Jönsson, H.O. di Rocco, Phys. Rev. A **43**, 4791 (1991)
23. B. Edlén, Metrologia **2**, 71 (1966)
24. S.P. Davis, M.C. Abrams, J.W. Brault, *Fourier transform spectrometry* (Academic Press, San Diego, Calif, 2001)
25. C. Yamada, H. Kanamori, E. Hirota, J. Chem. Phys. **83**, 552 (1985)
26. E.R. Peck, K. Reeder, J. Opt. Soc. Am. **62**, 958 (1972)
27. B.A. Palmer, R. Engleman, *Atlas of the Thorium spectrum* (National Technical Information Service, Springfield, VA, 1983)
28. E. Konz, T. Kraft, H.-G. Rubahn, Appl. Opt. **31**, 4995 (1992)
29. E.M. van Veldhuizen, F.J. de Hoog, J. Phys. D **17**, 953 (1984)
30. J.A. Aparicio, M.A. Gigosos, V.R. González, C. Pérez, M.I. de la Rosa, S. Mar, J. Phys. B **31**, 1029 (1998)
31. W.L. Wiese, J. Quant. Spectrosc. Radiat. Transfer **47**, 185 (1992)
32. A. Thorne, U. Litzen, S. Johansson, *Spectrophysics* (Springer-Verlag, Berlin, Heidelberg, 1999)
33. R.L. Kurucz, E. Peytremann, SAO Special Report 362 (1975)